ELSEVIER

Chemical Geology 175 (2001) 397–428

CHEMICAL GEOLOGY
INCLUDING
ISOTOPE GEOSCIENCE

www.elsevier.com/locate/chemgeo

Mantle reservoir geochemistry from statistical analysis of ICP-MS trace element data of equatorial mid-Atlantic MORB glasses

Robyn E. Hannigan [a,b,1], Asish R. Basu [a,*], Friedrich Teichmann [a,2]

[a] *Department of Earth and Environmental Sciences, University of Rochester, Rochester, NY, 14627, USA*
[b] *Department of Chemistry and Physics, Arkansas State University, State University, AR 72467, USA*

Received 29 September 1998; accepted 5 June 2000

Abstract

We report Inductively Coupled Plasma Mass Spectrometer (ICP-MS) trace element concentration data for 21 elements in 51 basaltic glasses recovered from 58 stations along a 1500-km segment of the equatorial mid-Atlantic Ridge (MAR; 5°N to 5°S). Isotope systematics of these glasses revealed mixing between two isotopically distinct (Schilling, J.-G., Hanan, B.B., McCully, B., Kingsley, R.H., 1994. Influence of the Sierra Leone mantle plume on the equatorial MAR: a Nd–Sr–Pb isotopic study. J. Geophys. Res., 99, 12005–12028.) HIMU and DM mantle sources. Trace element data presented here describe three distinct mantle reservoirs. Based on our new trace element data, we identified three, and possibly four, end-member mantle reservoirs beneath the equatorial MAR. HIMU-type signatures dominate the glasses from the northern equatorial MAR (5°N to 0°) with La/Ba, La/Th and rare earth element (REE) values similar to P-type mid-Ocean Ridge Basalts (MORB; 0.1, 9.11, $(La/Yb)_N = 5.5$, respectively). The basaltic glasses from the southern region (0° to 5°S) are mildly radiogenic in Pb and light REE depleted with N-type MORB trace element values for La/Ba, La/Th and REE (0.8, 40.0, $(La/Yb)_N < 0.6$, respectively). We estimate the mantle magma-source characteristics and identify the relative contributions of the mantle end-member components in the glasses erupted along the 1500-km transect using the trace element concentration data. Specifically, we recognize the presence of a statistically and geochemically distinct mantle reservoir depleted in Th and Ba relative to average depleted MORB between the Romanche and the Chain fracture zones.

To reach the full potential of this data set, we model mantle reservoir compositions using a modification of Q-MODE factor analysis. Multivariate classification and reduction of these data clearly distinguish trace element groups each reflective of mantle source heterogeneities present in this region of the MAR. Statistical analysis of these new trace element and available Nd–Sr–Pb isotope data for the same samples defines four statistically significant distinct end-member mantle components. The binary mixing model developed previously from geochemical data that invoked the mixing of two mantle reservoirs, HIMU and N-MORB, cannot adequately explain the variance in these trace element data. Incompatible element

* Corresponding author. Fax: +1-716-244-5689.
E-mail addresses: rhanniga@navajo.astate.edu (R.E. Hannigan), abasu@earth.rochester.edu (A.R. Basu).
[1] Fax: +1-870-972-3089.
[2] Current address: Gen-Keyes Str. 22, A5020 Saltzburg, Austria.

0009-2541/01/$ - see front matter
PII: S0009-2541(00)00335-1

concentrations and ratios best describe the modeled end-members reservoirs, which are HIMU (HPM), transitional N-MORB (TNM), depleted N-MORB (DNM) and an fourth incompatible element-enriched component (EPM). The statistically determined end-members explain 100% of the geochemical variance in the population but their modeled compositions may be related to process controlled variation. We clarify the relationship between statistical and geochemical reservoirs and conclude that a multiple mantle component model involving three of the identified reservoirs is clearly necessary to describe, specifically, the trace element characteristics of the equatorial mid-Atlantic MORBs. Our statistical methods yield tabulated trace element concentration data for each of these the modeled mantle components and provide insights into the MAR system, unavailable by any other technique, by allowing an estimation of the relative contributions of these end-member components in each of the 51 basaltic glass samples.

Keywords: Factor analysis; Trace elements; Mid-Ocean Ridge Basalts; Mantle heterogeneity components

1. Introduction

Isotopic and trace element studies of ocean basalts characterize the various mantle source reservoirs and describe oceanic lithosphere/asthenosphere and mantle plume interactions (e.g., Hanan et al., 1986; Hart and Zindler, 1989; Dosso et al., 1993; Kurz, 1993; Schilling et al., 1994; Basu and Faggart, 1996). For example, isotope ratios clearly discriminate between two geochemically distinct end-member mantle reservoirs along a large segment of the equatorial mid-Atlantic Ridge (MAR); these end-member sources are identified as depleted N-type Mid-Ocean Ridge Basalts (MORB) and a HIMU "Sierra Leone plume" (Schilling et al., 1994). Major and trace element studies of southern Atlantic MORB basalts indicate that N-type MORB basalt erupt along distinct ridge segments. Other ridge segments in the Atlantic Ocean close to this region show chemical signatures like that of P-type MORB and are associated with the Sierra Leone, Ascension, St. Helena, Tristan da Cuhna and Gough plumes or their respective tracks (Humphries et al., 1985). A recent study (Dosso et al., 1999) of the MAR at 10–31°N has further documented that the depleted mantle source of N-MORB was also inhomogeneous, showing isotopic variations almost as large as the difference between depleted and enriched mantle. In this study, we focus on the equatorial MAR from 5°N to 5°S. Within this study area (Fig. 1) along a 1500-km ridge section of the equatorial MAR, evidence for plume-ridge interaction includes Pb and Sr isotopes and La/Sm ratios (Schilling, 1991; Schilling et al., 1994). Isotopic studies of this equatorial region show

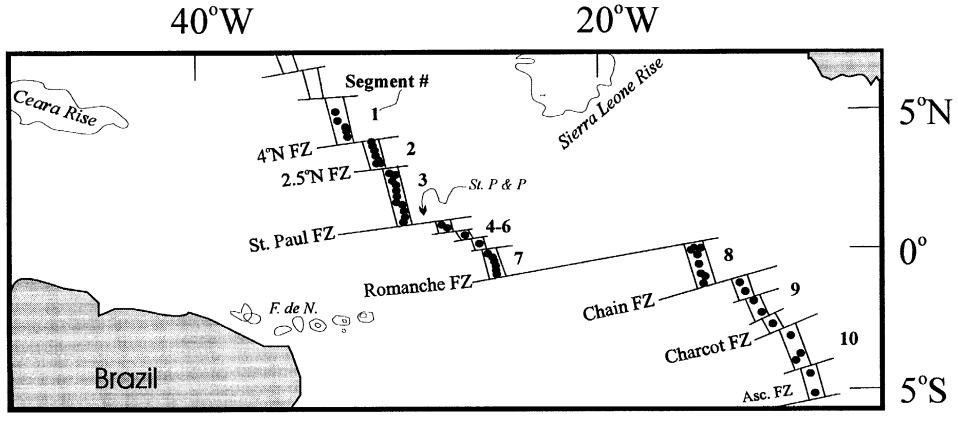

Fig. 1. Simplified morphotectonic map of the equatorial Mid-Atlantic Ridge (MAR) showing sample locations (open circles). Segment numbering used in text is shown after Schilling et al. (1994).

that a HIMU (P-type MORB) Pb-isotope anomaly centered around 1.7°N characterizes glasses from the northern segments (5°N to 0°). The position of this anomaly suggests that the Sierra Leone plume feeds the westward migrating MAR axis along a lateral sublithospheric channel (Schilling et al., 1994). Isotopic signatures characteristic of depleted N-type MORB dominate the southern (0° to 5°S) equatorial MAR. A region characterized by a modified P-type MORB isotopic signature occurs between the Romanche and Chain fracture zones suggesting the presence of a third "orphan" mantle component (Snow et al., 1993; Schilling et al., 1994).

In order to fully understand the geochemical cycles and the balance of trace elements in the upper mantle, we require additional information concerning the elemental composition of the different mantle reservoirs. The assessment of mantle magma mixing, based on the geochemistry of oceanic basalts, utilizes two very different approaches. The first uses elemental concentrations and isotopic ratios and simple binary or ternary magma mixing and modeling of modal, nonmodal and other complex melting processes. The second approach relies on physical and thermodynamic models of melt movement to explain the geochemistry of oceanic basalts. McKenzie and O'Nions (1991) developed a mathematical rare-earth element-inversion method, which attempts to reconcile both approaches and yields information concerning magma-source trace-element concentrations. To assess the geochemical signatures of the isotopically identified end-member mantle components beneath the equatorial MAR, we use trace element data obtained in our laboratory from the glass samples previously analyzed for major element and Pb, Nd and Sr isotopes by Schilling et al. (1994, 1995). Using incompatible trace element ratios, and, qualitatively, rare earth element (REE) patterns of the equatorial MAR glasses in conjunction with the Sr-, Nd- and Pb-isotopic data of Schilling et al. (1994), we describe the mantle magma-source trace-element concentrations and qualify the mixing relationships between the identified mantle components. We follow this description and interpretation of the MAR trace element data and develop a suite of statistical models to assess the conclusions drawn from trace element relationships and to elucidate relationships not apparent in traditional trace element data analysis. As shown by Fontignie and Schilling (1991), multivariate statistical analyses of trace element and isotopic data have the potential to provide significant insight into mantle-ridge systematics. We apply multivariate statistical modeling techniques to our equatorial MAR trace element data and available isotope data to statistically quantify the chemistry of the mantle reservoirs. We identify, quantitatively, geochemical characteristics of mantle components using standard factor analysis and then derive the reservoir trace element concentrations for the various mantle components via a modified Q-MODE factor analysis technique. We also provide relative proportion estimates of the different end-member mantle components in each of the basaltic glass samples.

2. Geochemical and tectonic setting

Recovery of fresh glassy pillow basalt samples was successful at 58 of the 59 stations dredged along a 1500-km portion of the MAR (5°N to 5°S) at 15- to 20-km intervals (Fig. 1). Schilling et al. (1994) provides a detailed sampling description covering the 51 samples from 10 segments (numbered 1 to 10 from north to south). Within this 1500-km-long profile, Schilling et al. (1994) distinguished two mixing zones in the mantle beneath this region of the MAR. These mixing zones are isotopically distinct with a gradational boundary between the Romanche and the Chain fracture zones. Isotopic signatures indicative of mixing between depleted asthenosphere and HIMU Sierra Leone plume mantle components, with the highest enriched-type MORB Pb-anomaly centered around 1.7°N, dominate the northern portion of the sampled region (segments 1 through 5). Glasses from southern segments 9 and 10 exhibit the signatures of depleted (and low radiogenic Sr) MORB, with a $^{87}Sr/^{86}Sr$ ratio of 0.7022 and a $^{143}Nd/^{144}Nd$ ratio of 0.5133 suggesting the presence of an N-type MORB end-member. Segments 6 through 8 show some isotopic enrichment, with the nature of their geochemical variations still under debate. These isotope data identify at least two, possibly three, geochemically distinct mantle components/reservoirs. Segments 9 and 10 show the most depleted signatures, which, most likely, represent the depleted asthenosphere or

a normal/depleted N-type MORB reservoir. Isotopically, glasses from segments 1 through 6 show the strong yet variable influence of the HIMU Sierra Leone plume. These basaltic glasses possibly result from mixtures between a depleted oceanic asthenosphere and an enriched mantle plume component. Glasses from segments 7 and 8 show an isotopic transition from N-type to P-type MORB, where a correlation between the degree of melting (7–10%; Schilling et al., 1994) and the Pb isotopes suggests preferential passive sampling of heterogeneous mantle components.

3. Analytical techniques

The major element analyses and isotope ratios for the equatorial MAR glasses have been reported by Schilling et al. (1994, 1995), and we present here the concentration data for 21 trace elements in the same samples (Table 1). Trace element concentrations for the 51 glass samples of Table 1 were obtained using the following procedure (Teichmann, 1995). Each sample represents 150 to 300 mg of hand-picked MORB glass. The trace elements and the REEs of the MORB glass samples were analyzed with a VG 2+ Quadrupole Inductively Coupled Plasma Mass Spectrometer (ICP-MS). Samples were digested in concentrated HNO_3 and HF in tightly sealed 15 ml Teflon TFE screw-cap bombs by heating on a hot plate for 24 hours. We performed all sample preparation in the Class 100 clean room at the University of Rochester; all acids were ultra-pure. The final solutions were prepared by adding the internal standard and diluting the sample with double distilled water. The composition of the internal standard was a 10 ppm solution of Ga, In, Cs, Bi and Re to correct for instrumental drift during the ICP-MS analyses.

Rare earths were corrected for interferences from BaO^+ and REE-O by an empirical table of ratios of BaO^+ and REE-O^+ interferences normalized to the $^{142}CeO^+$ oxide. Analytical precision is often $< 2\%$ of the reported concentration of the individual elements in Table 1. Precision of the analyses, as determined from duplicate analyses of the samples beginning with the original sample weighing, is generally $< 2\%$ for the REEs and $< 3\%$ for the other trace elements. We used BCR-1 (U.S. Geological Survey basalt) as the standard with its known concentration of the 21 trace elements used in this study (Table 1). We measured another rock standard as an unknown (USGS obsidian rock standard, NBS-287) to estimate the accuracy of the analytical procedure. We chose the BCR-1 and NBS-287 standards because the concentration of the trace elements in these rocks are well-known and our previous work supports the use of these standards in retaining accuracy and maintaining precision in our analyses. All sample concentrations reported in Table 1 are blank corrected (average of 20 blanks in ppm — Rb: 0.023, Sr: 0.025, Y: 0.0513, Ba: 0.043, La: 0.008, Ce: 0.022, Pr: 0.010, Nd: 0.006, Sm: 0.007, Eu: 0.008, Gd: 0.004, Tb: 0.006, Dy: 0.008, Ho: 0.005, Er: 0.007, Tm: 0.006, Yb: 0.004, Lu: 0.024, Pb: 0.004, Th: 0.007, U: 0.007). We found the published NBS-287 values for the trace elements and the REE concentrations to be within 2% to 3% of the analyzed results by our ICP-MS method using BCR-1 as the standard (percent standard error of 20 NBS-287 unknown runs — Rb: 1.7, Sr: 1.5, Y: 1.4, Ba: 1.2, La: 0.8, Ce: 0.9, Pr: 0.8, Nd: 1, Sm: 1, Eu: 1.2, Gd: 1.1, Tb: 1, Dy: 1.2, Ho: 1.4, Er: 1.4, Tm: 1.6, Yb: 1.2, Lu: 1.1, Pb: 2.4, Th: 2.1, U: 2.3). Thus, we are confident that the trace element analyses of MAR glasses, as reported in Table 1, have an overall precision and accuracy for a majority of the above elements much better than 3%.

4. Equatorial MAR glass trace element data

In this section, we present the trace element data and provide some general conclusions regarding mantle source reservoirs using the traditional trace element and combined isotope ratio approach. The equatorial MAR data show large variations in Ba, Rb, La, and Sr concentrations (Table 1). As expected for a relatively compatible element, the concentration of Y varies little. Zr exhibits slightly larger variations although not as prominent as those of Rb and Sr. Normalized trace element variations (Fig. 2) show a depleted pattern related to the N-MORB mantle component and an enriched pattern (E-MORB) related to the HIMU mantle component

Table 1
Trace element concentrations (μg/g) for 51 MORB samples from the equatorial Mid Atlantic Ridge. BCR-1 values from Tatsumoto et al. (1972) and Asmeron et al., 1994

Sample	Segment	Estimated distance along MAR (km)	Rb	Sr	Y	Ba	La	Ce	Pr	Nd	Sm
RC2806 55D-2g	1	10	2.94	125.5	26.2	36.8	5.30	14.6	2.11	11.2	3.43
RC2086 56D-3g	1	50	0.66	94.0	28.0	7.8	2.02	7.22	1.27	7.44	2.77
RC2086 57D-1g	1	75	2.00	118.7	31.4	23.2	4.10	12.5	1.94	10.7	3.54
RC2086 58D-1g	1	85	1.32	102.8	29.5	15.8	2.87	9.48	1.50	8.47	2.97
RC2806 59D-1g	1	95	1.62	100.2	34.9	18.8	3.69	12.3	2.00	11.5	3.95
RC2086 53D-4g	2	120	1.58	81.8	28.8	21.3	3.89	11.7	1.83	10.1	3.36
RC2086 54D-1g	2	130	0.97	75.8	28.0	12.1	2.68	8.85	1.47	8.26	2.86
RC2806 50D-1g	2	135	1.92	88.1	28.1	23.8	3.74	11.3	1.71	9.25	3.04
RC2086 49D-1g	2	155	0.65	89.8	28.5	7.0	2.06	7.25	1.23	7.00	2.50
RC2086 48D-9g	2	180	2.92	133.3	33.3	29.3	3.85	11.3	1.67	8.74	2.80
RC2086 47D-1g	2	210	2.55	97.3	36.7	32.9	5.04	14.9	2.28	12.4	4.28
RC2086 45D-1g	2	245	6.60	220.2	38.9	67.9	8.75	22.1	2.81	13.0	3.47
RC2086 44D-1g	2	245	1.60	95.3	24.3	19.8	3.03	8.95	1.37	7.54	2.60
RC2086 46D-1g	2	250	1.83	77.4	21.6	21.3	3.14	9.01	1.37	7.65	2.65
RC2086 42D-7g	3	340	7.76	161.8	23.8	109.2	10.70	25.1	3.12	14.5	3.77
RC2086 41D-1g	3	360	11.7	213.2	30.8	134.2	12.60	29.1	3.57	16.5	4.16
RC2086 40D-9g	3	390	18.7	349.9	27.8	214.1	19.70	43.4	4.93	21.0	4.60
RC2086 39D-1g	3	410	11.4	236.8	26.6	142.8	13.90	31.0	3.68	16.4	3.84
RC2086 38D-1g	3	435	3.57	171.0	24.6	34.6	4.07	10.7	1.47	7.51	2.29
RC2086 37D-1g	3	455	6.89	224.3	21.8	84.3	8.80	21.0	2.62	12.2	3.06
RC2086 36D-1g	3	470	5.79	172.7	28.0	64.6	7.08	17.5	2.27	11.0	2.99
RC2086 35D-1g	3	485	6.26	156.8	30.7	66.6	7.71	19.8	2.63	13.0	3.74
RC2086 35D-2g	3	485	5.89	146.8	29.7	64.5	7.56	18.4	2.46	11.8	3.27
RC2086 34D-1g	4	500	13.7	253.3	40.8	148.8	13.70	31.8	3.97	18.3	4.71
RC2086 33D-1g	4	505	15.9	233.3	47.2	136.3	14.00	33.1	4.17	19.3	4.90
RC2086 32D-1g	5	530	1.87	127.4	42.3	19.3	4.89	15.2	2.43	13.2	4.30
RC2086 31D-1g	6	565	3.03	128.4	48.6	29.4	5.95	17.5	2.67	14.3	4.65
RC2086 29D-3g	7	585	1.37	95.1	28.6	16.1	4.05	12.9	2.00	10.1	3.27
RC2086 26D-1g	7	640	1.33	148.0	52.0	12.5	5.66	18.8	2.95	15.6	4.67
RC2086 24D-1g	7	675	3.16	192.9	52.7	20.7	5.31	15.8	2.40	12.5	3.89
RC2086 23D-1g	7	705	2.18	177.7	45.4	17.0	4.10	13.0	2.02	10.9	3.48
RC2086 22D-4g	7	735	1.29	100.1	30.5	15.2	3.90	12.9	2.03	11.5	3.93
RC2086 21D-1g	7	750	1.55	149.6	44.5	12.0	3.57	11.9	1.89	10.6	3.48
RC2086 18D-1g	8	760	8.88	231.0	31.0	99.2	9.73	23.2	3.08	14.5	3.97
RC2086 7D-1g	8	775	16.9	447.4	25.0	205.4	17.80	39.1	4.78	20.9	4.82
RC2086 16D-1g	8	785	0.75	87.4	31.1	7.74	1.40	4.43	0.75	4.56	2.05
RC2086 8D-1g	8	795	4.33	169.5	30.8	54.2	5.99	16.0	2.31	11.7	3.68
RC2086 9D-3g	8	800	3.30	134.2	37.9	37.4	6.08	17.3	2.60	13.8	4.45
RC2086 10D-6g	8	830	2.68	132.5	36.2	27.5	4.73	13.9	2.12	11.4	3.72
RC2086 14D-2g	8	850	3.53	141.7	43.4	35.4	5.84	16.9	2.56	13.5	4.32
RC2086 11D-1g	8	865	1.72	126.6	25.7	20.5	3.09	9.2	1.39	7.5	2.51
RC2086 13D-3g	8	880	2.13	127.3	32.8	23.8	4.27	12.7	1.96	10.6	3.51
RC2086 12D-1g	8	910	2.30	149.8	30.8	28.9	4.74	14.2	2.12	11.4	3.63
RC2086 5D-1g	9	940	3.43	128.3	35.7	41.5	4.90	14.3	2.14	11.6	3.85
RC2086 4D-3g	9	975	16.1	340.9	28.6	234.5	13.10	29.6	3.64	16.3	4.03
RC2086 3D-2g	9	1065	5.37	133.3	30.7	63.5	6.02	16.0	2.28	11.8	3.70
RC2086 2D-1g	9	1070	0.34	111.2	23.4	4.45	2.14	7.62	1.27	7.31	2.59
EN061 2D-1Ag	9	1100	0.23	83.8	25.6	2.68	2.00	7.43	1.29	7.66	2.88
RC2086 1D-1g	10	1295	0.14	82.0	25.4	1.73	1.40	5.32	0.95	5.73	2.24
EN061 4D-1g	10	1430	0.52	89.8	29.5	6.46	2.48	8.91	1.50	8.68	3.15

(continued on next page)

Table 1 (*continued*)

Sample	Segment	Estimated distance along MAR (km)	Rb	Sr	Y	Ba	La	Ce	Pr	Nd	Sm
EN061 5D-1Ag	10	1440	1.56	88.9	36.8	16.4	2.98	9.44	1.49	8.45	3.13
BCR-1			47	330.0	39.0	678.0	25	53.6	6.9	28.6	6.55
NBS-287			127.5	63.5	38.0	894.0	31.72	63.36	7.38	27.24	5.57

Sample	Eu	Gd	Tb	Dy	Ho	Er	Tm	Yb	Lu	Pb	Th	U
RC2806 55D-2g	1.26	3.90	0.77	5.04	1.08	3.01	0.42	2.83	0.44	0.52	0.46	0.15
RC2086 56D-3g	1.04	3.48	0.69	4.55	0.99	2.81	0.40	2.68	0.42	0.26	0.09	0.03
RC2086 57D-1g	1.27	4.12	0.83	5.50	1.19	3.34	0.47	3.15	0.50	0.42	0.29	0.10
RC2086 58D-1g	1.08	3.63	0.71	4.67	1.02	2.91	0.41	2.84	0.45	0.36	0.17	0.06
RC2806 59D-1g	1.38	4.63	0.94	6.24	1.36	3.83	0.54	3.60	0.56	0.45	0.23	0.08
RC2086 53D-4g	1.19	4.11	0.83	5.53	1.21	3.43	0.49	3.31	0.52	0.40	0.27	0.11
RC2086 54D-1g	1.04	3.48	0.71	4.77	1.04	2.94	0.42	2.94	0.46	0.34	0.16	0.05
RC2806 50D-1g	1.09	3.64	0.73	4.95	1.08	3.06	0.44	3.02	0.48	0.36	0.29	0.09
RC2086 49D-1g	0.96	3.12	0.64	4.36	0.96	2.73	0.39	2.71	0.43	0.31	0.10	0.04
RC2086 48D-9g	1.03	3.36	0.66	4.39	0.97	2.73	0.39	2.70	0.43	0.38	0.32	0.11
RC2086 47D-1g	1.48	5.27	1.02	6.77	1.47	4.20	0.60	4.09	0.64	0.49	0.39	0.12
RC2086 45D-1g	1.21	4.01	0.75	4.82	1.06	2.99	0.42	2.91	0.45	0.99	1.00	0.33
RC2086 44D-1g	0.98	3.23	0.64	4.19	0.92	2.60	0.37	2.58	0.41	0.29	0.23	0.07
RC2086 46D-1g	0.97	3.27	0.64	4.32	0.94	2.64	0.37	2.47	0.39	0.35	0.22	0.07
RC2086 42D-7g	1.28	4.01	0.71	4.32	0.92	2.53	0.35	2.45	0.38	0.75	1.14	0.37
RC2086 41D-1g	1.39	4.60	0.81	5.15	1.08	3.00	0.42	2.76	0.43	0.89	1.32	0.41
RC2086 40D-9g	1.49	4.69	0.77	4.67	0.96	2.68	0.36	2.42	0.38	1.24	2.26	0.70
RC2086 39D-1g	1.34	4.01	0.70	4.22	0.90	2.48	0.34	2.32	0.37	0.86	1.54	0.49
RC2086 38D-1g	0.88	2.79	0.53	3.46	0.76	2.13	0.29	1.99	0.31	0.36	0.37	0.14
RC2086 37D-1g	1.14	3.28	0.58	3.60	0.76	2.10	0.29	1.95	0.31	0.63	0.92	0.30
RC2086 36D-1g	1.07	3.42	0.64	4.07	0.85	2.42	0.34	2.28	0.37	0.54	0.70	0.23
RC2086 35D-1g	1.29	4.25	0.81	5.20	1.11	3.11	0.44	2.90	0.46	0.58	0.80	0.26
RC2086 35D-2g	1.14	3.78	0.71	4.54	0.99	2.78	0.40	2.70	0.42	0.56	0.74	0.23
RC2086 34D-1g	1.54	5.17	0.94	5.94	1.29	3.67	0.52	3.61	0.57	1.01	1.65	0.53
RC2086 33D-1g	1.61	5.42	0.98	6.08	1.29	3.69	0.52	3.55	0.57	1.11	1.71	0.56
RC2086 32D-1g	1.49	5.22	1.02	6.66	1.47	4.12	0.59	4.04	0.63	0.57	0.30	0.10
RC2086 31D-1g	1.58	5.61	1.10	7.19	1.57	4.45	0.63	4.31	0.68	0.63	0.48	0.16
RC2086 29D-3g	1.36	4.56	0.74	4.83	1.06	3.03	0.51	3.59	0.46	0.54	0.22	0.09
RC2086 26D-1g	1.66	5.65	1.03	6.57	1.42	4.06	0.58	3.98	0.63	0.76	0.22	0.09
RC2086 24D-1g	1.40	4.58	0.84	5.65	1.19	3.40	0.49	3.41	0.55	0.65	0.37	0.16
RC2086 23D-1g	1.29	4.15	0.78	5.25	1.10	3.16	0.45	3.08	0.49	0.54	0.23	0.09
RC2086 22D-4g	1.37	4.92	0.95	6.18	1.33	3.81	0.54	3.66	0.58	0.51	0.19	0.07
RC2086 21D-1g	1.28	4.24	0.82	5.52	1.16	3.35	0.48	3.26	0.53	0.45	0.18	0.07
RC2086 18D-1g	1.34	4.21	0.77	4.66	1.03	2.84	0.40	2.71	0.43	0.93	1.04	0.34
RC2086 7D-1g	1.61	4.52	0.73	3.98	0.81	2.12	0.28	1.88	0.29	1.29	2.11	0.67
RC2086 16D-1g	0.87	2.98	0.64	4.41	1.02	2.93	0.43	3.01	0.49	0.18	0.10	0.03
RC2086 8D-1g	1.29	4.18	0.78	4.86	1.07	2.92	0.42	2.86	0.45	0.66	0.54	0.18
RC2086 9D-3g	1.52	5.16	0.99	6.50	1.39	3.91	0.55	3.69	0.60	0.61	0.47	0.17
RC2086 10D-6g	1.29	4.40	0.84	5.56	1.20	3.38	0.47	3.26	0.52	0.52	0.35	0.12
RC2086 14D-2g	1.50	5.19	0.99	6.43	1.41	3.96	0.56	3.90	0.61	0.68	0.46	0.15
RC2086 11D-1g	0.97	3.09	0.60	3.93	0.85	2.42	0.34	2.39	0.37	0.35	0.21	0.07
RC2086 13D-3g	1.26	4.23	0.81	5.31	1.15	3.24	0.46	3.09	0.48	0.48	0.29	0.10
RC2086 12D-1g	1.35	4.39	0.83	5.43	1.15	3.24	0.45	3.02	0.47	0.51	0.34	0.12
RC2086 5D-1g	1.41	4.84	0.94	6.16	1.32	3.76	0.53	3.44	0.53	0.48	0.40	0.13
RC2086 4D-3g	1.42	4.24	0.71	4.30	0.91	2.46	0.34	2.32	0.35	1.03	1.42	0.42
RC2086 3D-2g	1.32	4.31	0.83	5.32	1.16	3.25	0.46	3.10	0.49	0.54	0.56	0.17
RC2086 2D-1g	0.98	3.17	0.62	4.07	0.89	2.51	0.35	2.36	0.37	0.29	0.07	0.04
EN061 2D-1Ag	1.08	3.63	0.71	4.72	1.03	2.89	0.42	2.81	0.44	0.30	0.06	0.03

Table 1 (*continued*)

Sample	Eu	Gd	Tb	Dy	Ho	Er	Tm	Yb	Lu	Pb	Th	U
RC2086 1D-1g	0.86	2.98	0.61	4.14	0.90	2.53	0.36	2.42	0.38	0.24	0.04	0.02
EN061 4D-1g	1.15	4.03	0.80	5.37	1.17	3.35	0.48	3.23	0.51	0.36	0.10	0.04
EN061 5D-1Ag	1.10	4.07	0.83	5.63	1.26	3.64	0.52	3.49	0.56	0.38	0.19	0.07
BCR-1	1.92	6.82	1.05	6.37	1.34	3.71	0.54	3.39	0.49	13.56	5.98	1.72
NBS-287	0.78	5.51	0.95	6.21	1.36	4.03	0.64	4.33	0.70	16.7	12.6	4.64

NBS-287 values from Hollocher, 1993.

(Schilling et al., 1994). Some samples are plotted in regions either bounded by these two reservoirs or beyond, implying the presence of a third mantle component and mixing between these reservoirs. The largest variation in concentration occurs in the incompatible elements where Ba, Rb and Sr vary as much as three orders of magnitude from primitive mantle. The depleted N-type MORB patterns of the glasses from the southern segments (0° to 5°S, segments 8–10 in Fig. 1) show an incompatible element depletion similar to other MORB patterns (Sun, 1980; Saunders and Tarney, 1984; Wilson, 1989; Dosso et al., 1993). The incompatible element-enriched, E-MORB patterns of samples from the northern segments resemble the smooth convex trace element patterns typical of ocean island basalts (Sun, 1980; Wilson, 1989; Watson, 1993; Watson and McKenzie, 1991), although some samples from segments 2, 3, 4, 8, and 9 show variations beyond the normal E-MORB pattern (Fig. 2).

REE abundance patterns of Fig. 3 describe the variation in REE abundances from North to South along the 1500-km ridge section. Overall, the samples show very smooth REE patterns. The REE concentrations in the glasses range from depleted $[(La/Yb)_N = 0.5]$ to enriched $[(La/Yb)_N = 2]$. None of the samples show any discernable Eu anomaly. In general, the REE patterns mimic the patterns of depleted N-type MORB and E-MORB with several samples falling in a region beneath these two common end-members (Fig. 3). The REE concentrations of the glass samples falling close to these two end-members may reflect either mixing of the two mantle reservoirs prior to eruption or the sampling of a third mantle component as indicated by the isotope data. The REE data clearly support conclusions drawn from isotopic studies (Schilling et al., 1994) that there is more than one geochemically distinct mantle source beneath the equatorial MAR.

4.1. Trace element evidence for multiple end-member compositions

Trace element data are useful in the identification of mantle components such as depleted asthenosphere and P-type MORB (e.g., Michael, 1995; Niu and Batiza, 1995). Specifically, for petrogenetic studies, which utilize Pb-isotopes (such as in the case of the equatorial MAR), the Th–U ratio of depleted oceanic asthenosphere is extremely useful in the identification of mantle reservoirs. The data presented here show a strong correlation between Th and U ($r^2 = 0.997$; $\alpha = 0.05$). Based on this relationship, we estimate the average N-MORB reservoir U/Th in the equatorial MAR value as 2.46 and the average HIMU reservoir U/Th value as 3.13. Sm and Eu also show a strong correlation ($r^2 = 0.964$; $\alpha = 0.05$) in these data. The strong correlation between Sm and Eu indicates that little or no low pressure fractional crystallization of plagioclase occurred since Eu is more compatible than Sm in plagioclase. Plagioclase fractional crystallization is also discounted due to the absence of negative Eu anomalies, or Eu/Eu^* values significantly less than 1. FeO–MgO relationships show no olivine or clinopyroxene control. Schilling et al. (1995) showed that, in the case of the equatorial MAR, there is no justification for the normalization of data to a constant MgO = 8.0. These authors also showed that the glass major element data show variations quite dissimilar to the global population described by Klein and Langmuir (1987). Although N-MORB and HIMU are sampled in different thermal environments and the U/Th ratios may reflect source and fusion conditions, we do not normalize our trace element data to

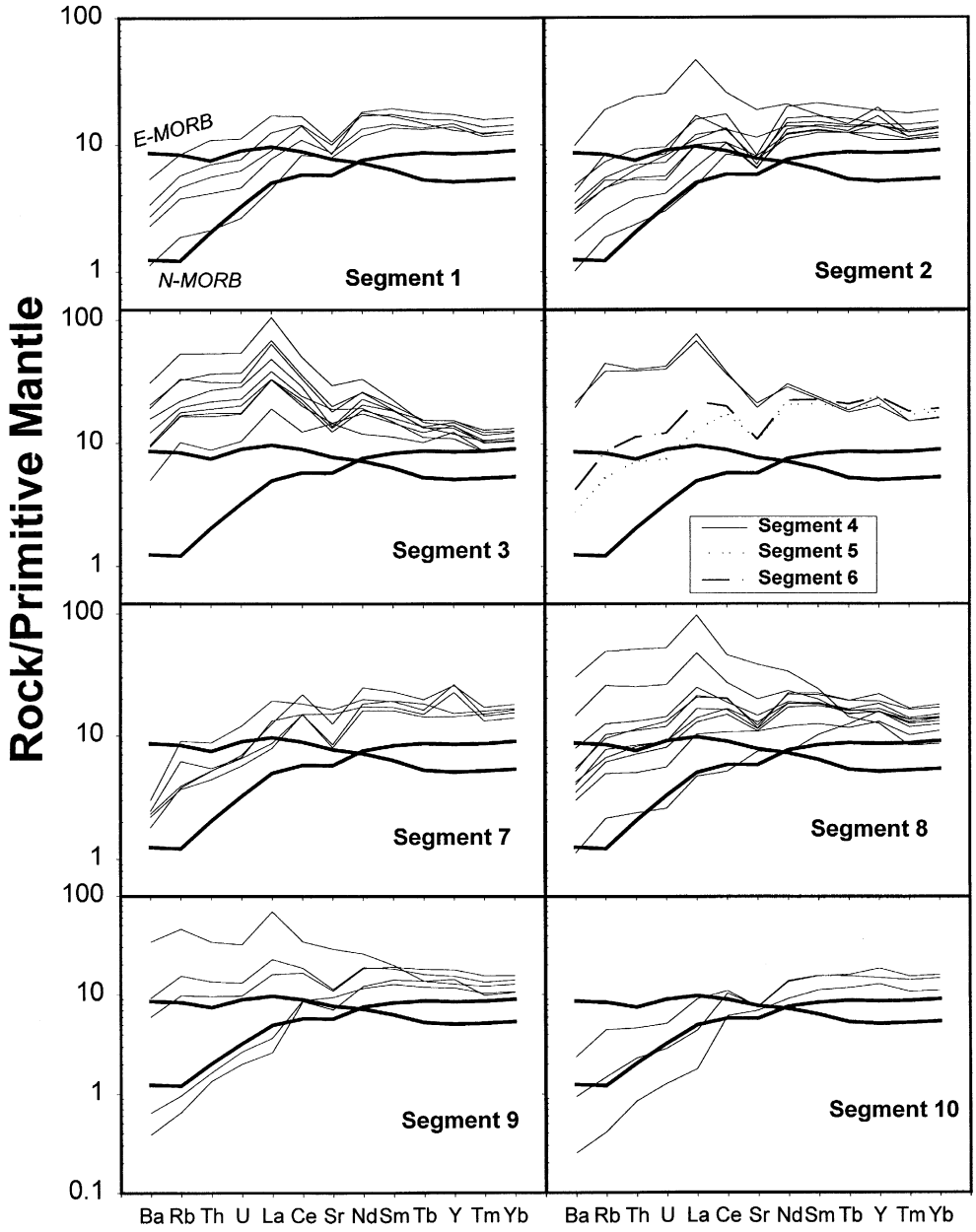

Fig. 2. Normalized trace element concentration patterns for 51 MORB glass samples analyzed in this study. The data are compared with the E-MORB (Sun and McDonough, 1989) and N-MORB (McDonough, 1996 — http://www.EarthRef.org/GERM/reservoirs/morb8.html) end-member. Normalization values from McDonough and Sun (1995) and McDonough (1998).

a constant MgO value. In this study, we assume no garnet control based on the Schilling et al. (1994) study, which indicated that the decompressional melting of the mantle N-MORB source began within the spinel stability field at 13 to 18 kbar.

The five light-REE (LREE) depleted samples from segments 9 and 10 represent the most depleted MORB (Fig. 3). Their $(La/Sm)_N$ ratios range from 0.39 to 0.6, well below the LREE depletions observed in MORB samples from other regions of the

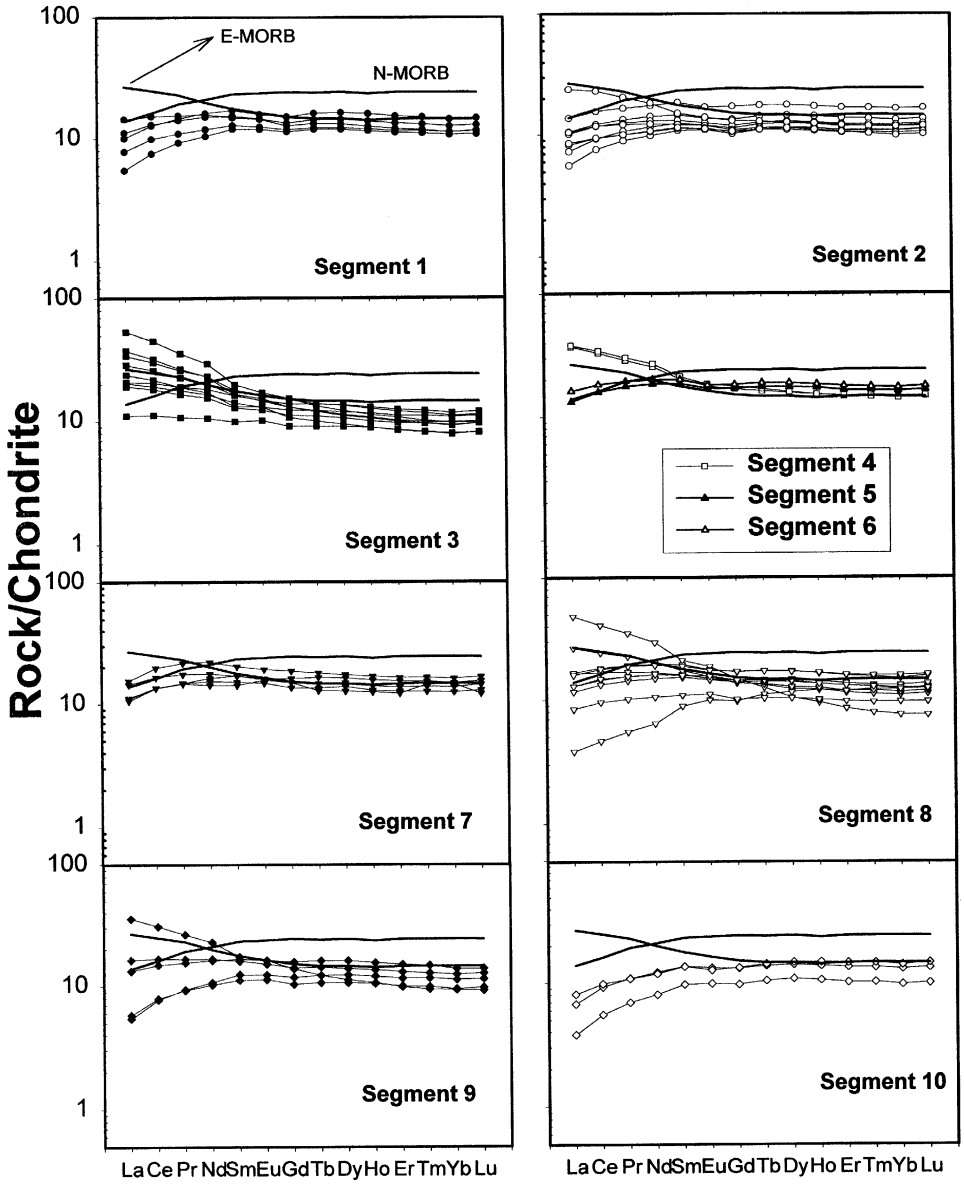

Fig. 3. Normalized REE patterns for the 51 samples arranged by segments. Each segment allows a relative comparison with the two generally defined end-members, E-MORB and N-MORB. Note that the most depleted N-type MORB REE patterns occur in segment 10 and that segment 8 shows strong signatures of both an enriched and depleted source. Normalization values for chondrites are from Anders and Grevesse (1989).

Atlantic, which generally range between 0.7 and 0.8 (Schilling et al., 1994). Samples from the region closest to the 1.7°N Pb-isotopic anomaly (segments 1–6) show trace element concentrations similar to P-type MORB with an average $(La/Sm)_N$ ratio of 1.8. The composition of P-type MORB basalts varies with specific plume compositions as well as with the amount of interaction between the plume and de-

pleted lithosphere/asthenosphere. As expected for the equatorial MAR samples from the northern portion of the MAR (5°N to 0°), the glasses show increased incompatible element concentrations.

4.2. Multiple mantle magma reservoirs beneath the equatorial MAR

Overall, the trace element compositions of all 51 glass samples can be explained in terms of mixing between the N-MORB and HIMU end-member reservoirs. We use La/Th and La/Ba relationships to explore the reservoir mixing relationships beneath the equatorial MAR. Th, a high-field strength element (HFSE), and Ba, a large ion lithophile element (LILE), are often used in petrologic modeling of igneous systems. The high charge and relatively smaller size of Th result in its incompatibility in most major mineral phases. Although Ca-pyroxene can fractionate the HFSE from one another, there is no evidence to suggest that crystal fractionation of pyroxene fractionates La from the Th (Forsythe et al., 1994). Using the "incompatible" element ratios La/Th and La/Ba of the equatorial MAR glasses (Fig. 4), useful insights are gained into the relative causes of mantle geochemical heterogeneity beneath the MAR. The differences in La/Th and La/Ba observed along the length of the MAR requires that the mantle reservoirs beneath this region be heterogeneous in composition because neither partial melting nor fractional crystallization are expected to have a significant effect on the La/Th and La/Ba values.

The majority of samples from northern segments 1 and 2 are more depleted in highly incompatible elements than average depleted N-type MORB (Fig. 4). Incompatible element-enriched MORB (EM) do not show depletions in Th and have relatively constant La/Th ratios (Fig. 4a; average enriched MORB La/Th ≅ 9.1). In contrast to the constant La/Th ratio in EM, depleted N-type MORB always have higher and more variable La/Th ratios. In general, samples from the southern segments 7 through 10 show the depleted La/Th N-type MORB signature (Figs. 4a and 5). As shown in Fig. 4, Th and Ba display similar variability with respect to La. Note, however, that samples from segment 7 and, to some degree, those from segment 8 (Fig. 4) do not fall along the expected hyperbolic mixing trajectory between the N-MORB and E-MORB mantle reservoirs. This observation hints at trace element heterogeneity in the magma-source reservoirs beneath this region and also at the presence of a third mantle component in addition to the N-MORB and E-MORB components.

If there is a third "orphan" mantle component beneath the equatorial MAR with low Ba (compared to N-MORB) concentrations as suggested above (Fig. 4b), is this component also anomalously depleted in Th relative to N-MORB? If heterogeneity among the sources is the cause of the La/Th and La/Ba mixing relationship of Fig. 4, and if we accept that the bulk of the MAR samples are depleted in Ba compared to E-MORB (Fig. 4b), we must establish that the sole cause of this variation is attributable to source heterogeneity. To address this issue, we compare the equatorial MAR basalts from individual ridge segments on the basis of La and Th concentrations. We plot the La vs. Th concentrations (Fig. 5) and compare them to the E-MORB line defined as La = 9.1 Th (similar to the calculation and comparison of La/Ta by Bach et al., 1996). Depleted N-type MORB usually have higher and more variable La/Th ratios as shown by the glasses (Fig. 5b) from the southern segments (segments 9 and 10). The glasses from the northern segments, described above and by Schilling et al. (1994) as mixtures of the depleted asthenosphere and HIMU (Sierra Leone plume) mantle reservoirs, have lower La/Th ratios (Fig. 4a) consistent with the contribution of HIMU melt to the erupting asthenospheric magma. Glasses from the southernmost segments 9 and 10, described above as dominantly depleted N-type MORB, show variable but high La/Th ratios (Fig. 4a). Of interest are the glasses from segments 7 and 8, which follow a general trend defined by the line La = 19.8 Th in Fig. 5b. These samples show La–Th relationships similar to the La–Ta variations observed in basalts from the North Chile Ridge (Bach et al., 1996). Melt-peridotite reactions cannot account for the observed Ba and Th depletions in segments 7 and 8 (Figs. 4 and 5) since these elements do not generally fractionate from each other during melting (Forsythe et al., 1994). There is also no evidence to support Ba–Th fractionation due to magma-differentiation

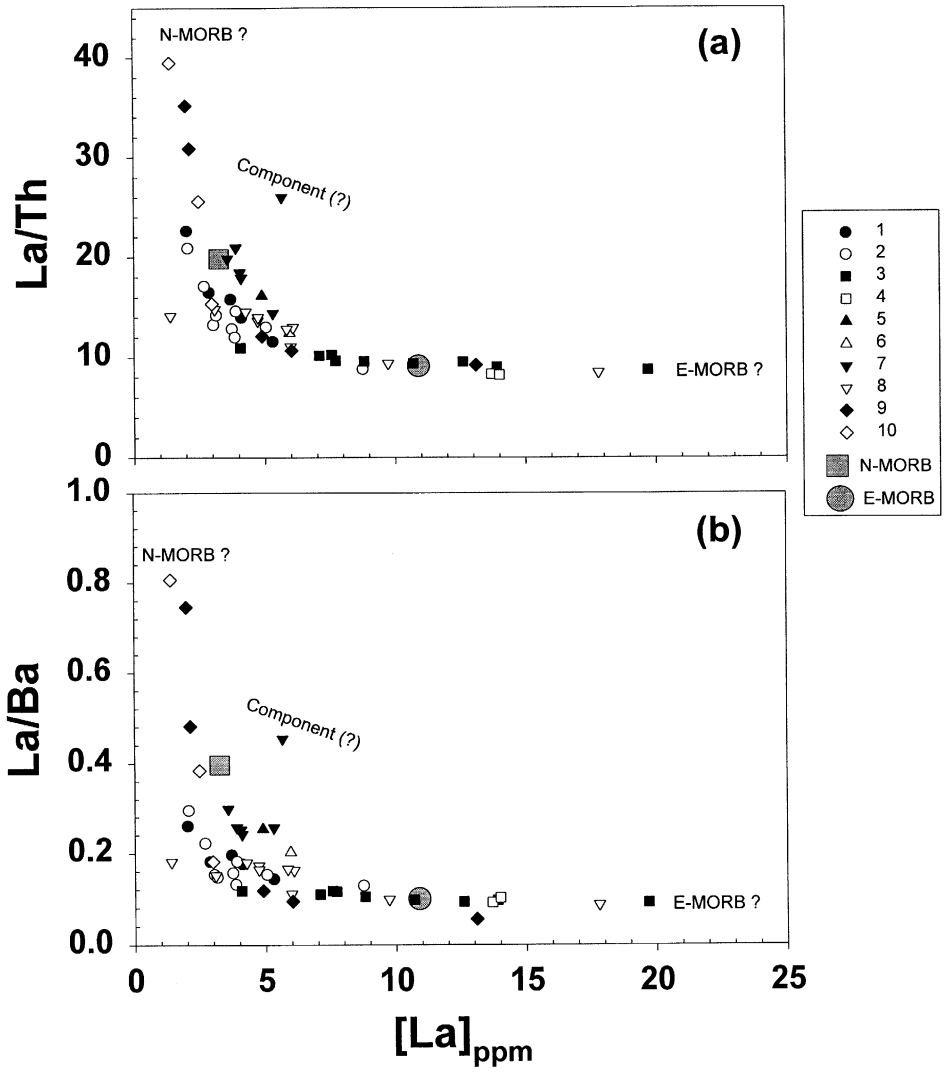

Fig. 4. La–Th and La–Ba relationships clearly show the relative influence of the N-MORB and E-MORB components. Northern segments are enriched in Th with southern segments showing Th and La depletion. The La–Th relationships of segments 1 and 2 show significant Th depletion related to a mantle component distinct from N-MORB and E-MORB. Suspect components are indicated as well as generalized values of E-MORB and N-MORB from the literature.

processes such as fractional crystallization (Johnson et al., 1995; Bach et al., 1996). We contend that the low Ba and Th concentrations are characteristic of the mantle source beneath segments 7 and 8 in the mid-Atlantic region. We assert that the source depletion occurred during earlier melting episodes associated with the formation of oceanic crust along the MAR as suggested in the case of the North Chile Ridge (Bach et al., 1996). These incompatible element depletions are a local characteristic of the upper mantle beneath these segments of the equatorial MAR, perhaps related to the development of the Romanche and Chain fracture zones (Fig. 1).

La/Ba and La/Th variations between the segments as described above (Figs. 4 and 5) are also supported by the isotopic variations of Nd, Sr, and

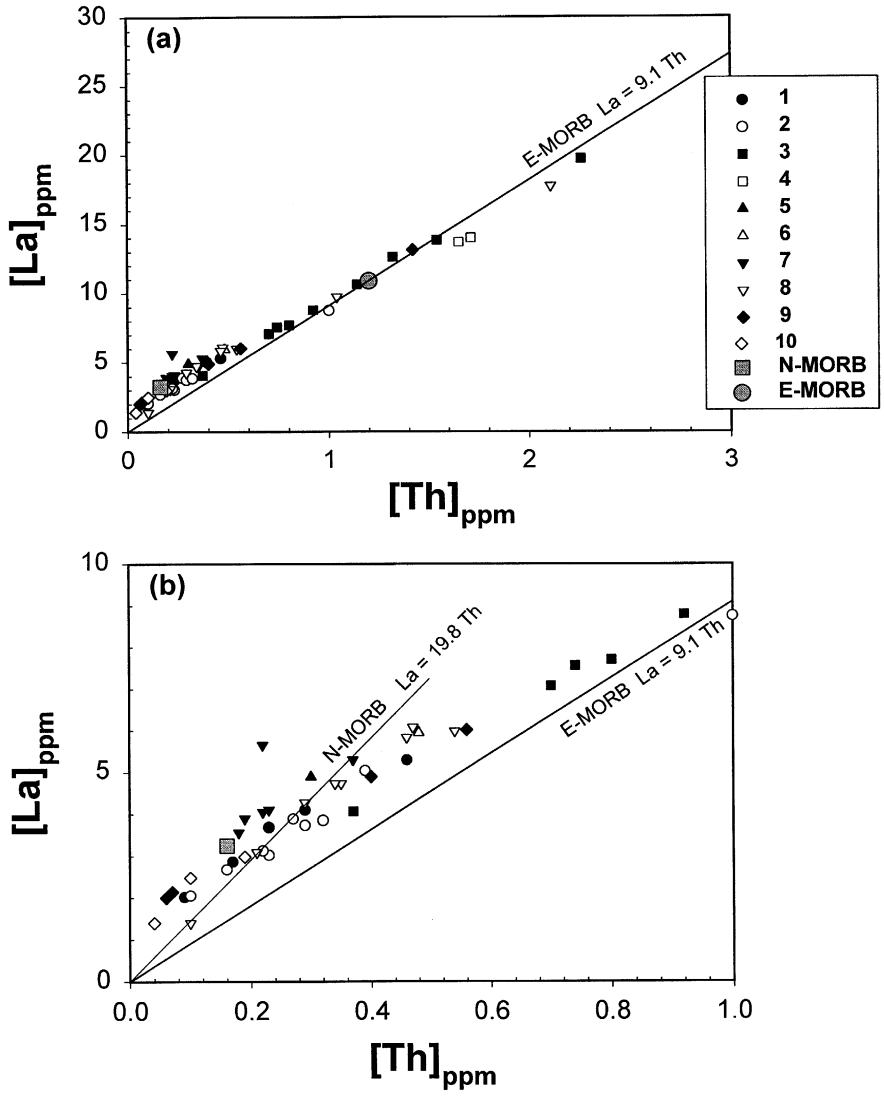

Fig. 5. The relationships between [La] and [Th] on a segment-by-segment basis show the presence of three, possibly four, end-members in the equatorial MAR. The enriched MORB regression line (La = 9.1 Th) is shown for comparison. Most of the southern segments fall along a line defined by mixing between two depleted end-members such as depleted asthenosphere and the third component. Samples fall below and above the enriched MORB regression line suggesting the presence of mantle components distinct from depleted MORB and E-MORB.

Pb (Schilling et al., 1994). La/Ba and La/Th vs. Sr-, Nd- and Pb-isotopes generally fall along a mixing trajectory between an enriched-mantle, HIMU and N-MORB reservoirs (Fig. 6). There appears to be a slightly different trend defined by glasses from segments 7 and 8 where the isotopic signature is constant over a range in La/Ba and La/Th values. There is no evidence, contrary to the suggestion of Snow et al. (1993), for secondary seawater alteration in this probable third depleted MORB reservoir in our study area as indicated by their generally lower $^{87}Sr/^{86}Sr$ ratios. We contend that these trace element–isotope relationships of Fig. 6 combined with the relationships discussed above clearly indicate the

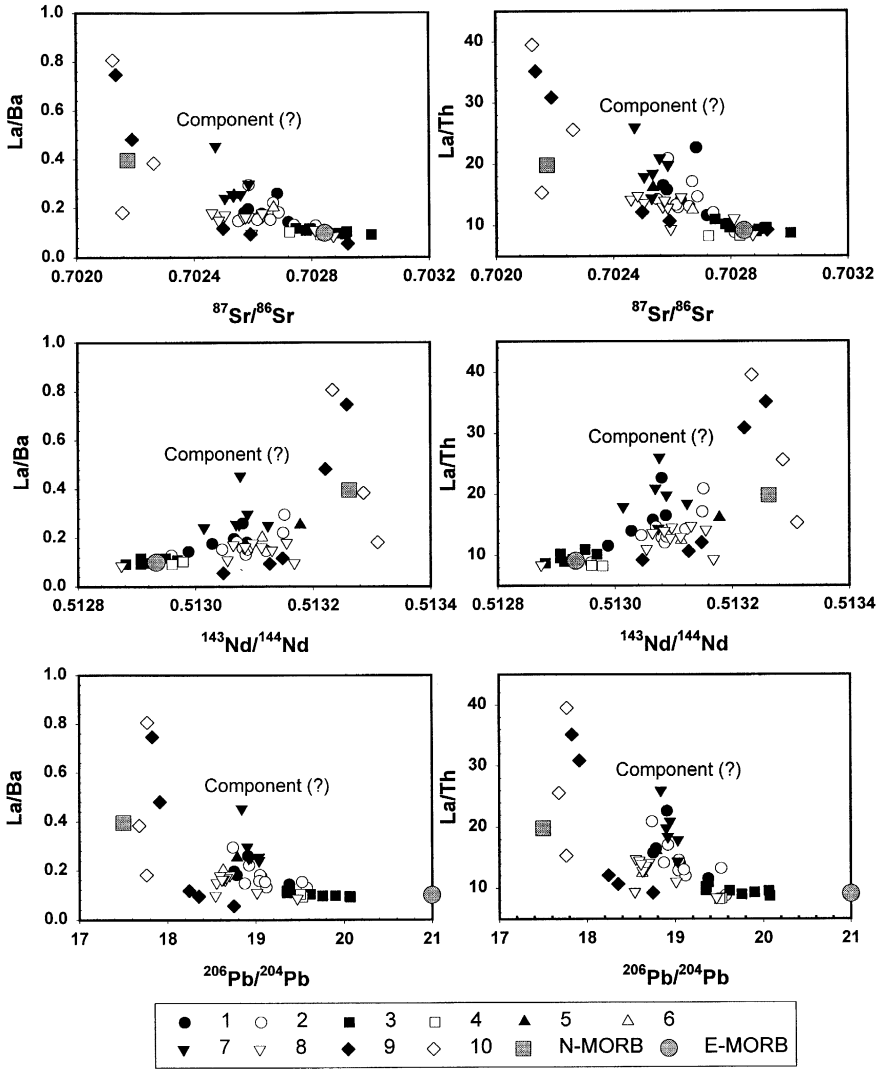

Fig. 6. Sr-, Nd- and Pb-isotope data (Schilling et al., 1994) of the analyzed samples compared to their La/Ba and La/Th. The relationships clearly indicate more than three components. In particular La/Th-isotope relationships define the presence of the third component located near segments 7 and 8.

presence of a third component depleted in Ba and Th. This incompatible element depleted source is very likely a local but not unique phenomenon. Similar depletions occur in basalts from the EPR seamounts and the North Chile Ridge (Niu and Batiza, 1995; Bach et al., 1996).

In summary, the MAR glass trace element data indicate the following concerning the probable mantle source reservoirs beneath the equatorial MAR. The majority of samples follow the binary mixing trend between an enriched, HIMU mantle component and depleted suboceanic asthenosphere. Evidence for the presence of a third geochemically distinct mantle component occurs in glasses from segments 7 and, most strongly in segment 8.

We suggest that the La/Ba and La/Th ratios in the 51 basaltic glass samples of our study are primarily controlled by suboceanic asthenosphere composi-

tion with a major contribution, overall, from the HIMU mantle reservoir and variable contributions from a minor, third mantle end-member. In general the La/Th and La/Ba relationships corroborate the isotope results, which show that the strongest Sierra Leone plume signature occurs in the northernmost segments (Schilling et al., 1994). Depleted asthenosphere signatures occur along the southern segments. Again, the presence of a third distinct component in this region is seen in the individual segments (Figs. 4–6). Although isotope data suggests its presence, the trace element relationships of the analyzed basaltic glasses clearly show a third reservoir depleted in Ba and Th located in the region between the Romanche and Chain fracture zones (Fig. 1).

The above results support passive sampling of a heterogeneous mantle region, which is volatile element and radiogenic Pb-enriched. This "lumpy" mantle region (Schilling et al., 1994) preferentially melts during mantle decompression. The depletions in Ba and Th in the area south of the St. Peter–St. Paul region (Fig. 1) along the MAR indicate a relatively long-lived third mantle component, geochemically distinct from N-MORB and P-MORB (HIMU).

It is important to note that while the incompatible element ratios of the glasses show compositional variation indicative of multiple mantle reservoirs, there is not a one-to-one mapping correlation between source and melt. Fractionation occurs even among the highly incompatible element concentration ratios during partial melting. The effect of this fractionation is variable as in the case of Ce/Pb and La/Ba, which are fractionated differently depending on the amount of sulfide and plagioclase precipitation, both of which crystallize in MORB (Sims and DePaolo, 1997). We address, statistically, the process related variation below.

5. Statistical methods

Using a modified Q-MODE factor analysis of the trace element data (Table 1) and the available geochemical data on the major elements (Schilling et al., 1995) of the same 51 samples, we attempt below a statistical modeling of the mantle reservoir compositions for the equatorial mid-Atlantic MORB. The geochemical data sets for the equatorial MAR satisfy the following criteria necessary for statistical modeling: sample size is large enough to accurately represent the entire population of MORB glasses erupting along the equatorial MAR; field relationships for all of the samples are well constrained; and complete petrologic information for each sample is available. For the purposes of this study, each glass sample is described by the following geochemical variables:

6 Major elements (Schilling et al., 1995): Al_2O_3, FeO_T, MgO, CaO, Na_2O, TiO_2;
14 REE: La, Ce, Pr, Nd, Sm, Eu, Gd, Tb, Dy, Ho, Er, Tm, Yb, Lu;
3 Low-field strength elements (LFSE): Rb, Ba, Sr;
4 High-field strength elements (HFSE): Y, Pb, Th, U;
3 Isotopic ratios (Schilling et al., 1994): $^{206}Pb/^{204}Pb$, $^{87}Sr/^{86}Sr$, $^{143}Nd/^{144}Nd$;
4 Trace element ratios: Ce/Pb, U/Th, La/Ba, La/Th;
3 Derived variables: $(La/Sm)_N$, $(La/Yb)_N$, Eu/Eu^*.

5.1. Nonparametric statistical techniques

Geochemical analysis transforms the chemical composition of equatorial MAR basaltic glasses into a vector of numbers. Fontignie and Schilling (1991) and Schilling et al. (1994) examined similar glass data in a variety of ways ranging from traditional graphical techniques (e.g., binary mixing diagrams) to elementary statistical techniques such as regression to parametric multivariate techniques such as principal components analysis (PCA).

The equatorial MAR data are an example of a nonnormal population containing more than one subpopulation. Mixing of a variety of magma reservoirs prior to eruption presumably produced the subpopulations identified by isotope ratios (Schilling et al., 1994). Although the use of nonparametric statistics pervades sedimentology, there are only a few examples (Miesch, 1976; Leinen and Pisias, 1984) of the use of nonparametric statistics in the study of igneous petrogenesis.

We begin our statistical exploration of the equatorial MAR data set with the nonparametric Spearman rank correlation coefficient (SRCC) using the Statistical Package for the Social Sciences (SPSS; Norušis, 1997; see Appendix A). Compositional variation in most MORB basalts results from a combination of physical and chemical processes including fractional crystallization, assimilation, partial melting and magma mixing. SRCCs detect each of these processes as they have a characteristic effect on the final composition of a sample and may generate unique interelement correlations. For example, if fractional crystallization occurred within a magma reservoir, in isolation from other processes, all interelement SRCCs would be $+1$ or -1. This relationship holds true unless changes in the mineral phases from the melt cause reversals in the enrichment and depletion trends, or where several samples have the same composition for one or more variables (tied observations; Rock, 1988). The combination of two or more processes should generate the population estimator $|\rho| < 1$. For our purposes, we considered only $|\rho|$ values greater than 0.80, which remove confounding process effects.

5.2. "*Robust*" *parametric statistical techniques*

Most geological data are nonnormally distributed. Many statistical techniques, however, are available that address the violation of the normality assumption and still provide accurate statistical parameters for a population of data. In this study, we applied robust parametric statistical techniques to the equatorial MAR data to further elucidate relationships within the data related to magma mixing and mantle source heterogeneity. We applied only those parametric techniques known to be resistant to the violation of the normality assumption.

5.2.1. *Cluster analysis*

Cluster analysis includes an assortment of techniques that perform classification by assigning observations to groups so that each group is more or less homogeneous and distinct from other groups (Davis, 1986; see Appendix A). This method provides detailed insight into significant relationships between samples, and for our purpose yields important information about the end-member populations.

5.2.2. *Discriminant analysis*

Earth science widely employs discriminant functions for the statistical analysis of geochemical data because of their power as a statistical tool and their ability to treat either univariate or multivariate data (Davis, 1986). For this study, we used the multivariate form of the discriminant function (see Appendix A). In *N*-dimensional space, this function maximizes the separation between 2 or more groups of data. This technique also maximizes the correspondence between the a priori groups and the statistical groups. Successful analysis reproduces the a priori groups with close to 100% accuracy. Correct classification of samples into groups also allows placement of previously unclassified samples.

5.2.3. *Factor analysis*

In order to determine the trace element compositions of the end-members identified using cluster and discriminant analysis, we chose a modified factor analysis approach. This robust technique allows violation of the normality assumption without a significant increase in error. Sedimentologists have long used end-member compositional modeling based on multivariate statistical analysis (Leinen and Stakes, 1979; McMurty et al., 1981). This technique, when applied in a simplified form (PCA) to basalt trace element data, can yield significant information concerning mantle heterogeneity (Fontignie and Schilling, 1991). To determine the number of end-member components, the technique uses extended Q-MODE factor analysis (Miesch, 1976) to identify the principal sources of variation within the data set.

Standard Q-MODE factor analysis, however, fails to provide a direct solution to the magma-mixing problem common in igneous systems. This is because the vectors generated by standard factor analysis are not composition vectors. These vectors thus provide no information on the absolute composition of end-members. Similarly, the factor scores only give a relative measure of the importance of each variable in each end-member. The extended Q-MODE technique used here addresses these problems since the data are "closed" by summing the variables for each sample to a constant value (Miesch,

1976; Leinen and Pisias, 1984). A closed data set allows calculation of the absolute abundance of each end-member factor in each sample. A common consequence of the closing of the data is negative values in the factor loading matrix. "Varimax" rotation eliminates this problem. This rotation ensures that the absolute abundance of each end-member factor in each sample is greater than or equal to zero. Another positive outcome of varimax solutions is that the factors are orthogonal (statistically uncorrelated). The relationships among the observations are not changed by rotation, although the position of the individual objects within the space defined by the factor axes is altered. After rotation, positive or zero contributions of the end-member factors describe all of the samples. Varimax rotation of a data set in which the sum of the variables in each sample is constant results in a factor analysis, which describes each sample in terms of the absolute abundance of end-member factors whose compositions are given in the concentration units of the original data.

The goodness-of-fit measure for the extended factor model defines the degree to which the modeled factors explain the variance of the data set. We use the goodness-of-fit statistic known as the coefficient of determination (COD: r^2). This statistic should not be confused with the sample SRCC defined above. The COD is defined as:

$$r_j^2 \approx \frac{s(x)_j^2 - \left(d_j^{**}\right)^2}{s(x)_j^2},$$

where d_j^{**} is the standard deviation of the factor model residuals and $s(x)_j^2$ is the variance of the jth column of the original data matrix (Miesch, 1976). If the model explains all of the data perfectly, all values of d_j^{**} and r_j^2 are unity.

Chayes (1960) suggested that if the row-sums of the data matrix are constant across all rows, each variable must show a negative correlation with at least one of the others, even if the variables have no genetic relationship. The key question, however, is to what degree the constant row-sum constraint influences the configuration of the factor–variance relationships. Chayes (1960), Chayes and Kruskal (1966) and Miesch (1976) show that the effect of the constant row-sum constraint is negligible.

Intensive variables, where the relative concentration of each element in a system such as the equatorial MAR is a proportion of the whole, are common in geochemistry and petrology. When these variables describe the geochemical composition of rocks, they represent projections of the extensive quantities (reservoir source composition) onto the unit hyperplane in geochemical hyperspace. The projection of extensive variables into intensive space leads to the intensive properties of each variable summing to one and therefore constitutes a closed array (Stanley, 1990). Rock compositions, whether expressed in geochemical concentration or modal mineralogy terms, are subject to a loss of a degree of freedom due to their expression as proportions. In order to avoid this loss, unbiased statistical analysis of rock compositions requires the use of compositional variables that are unaffected by array closure. Ratios of the component proportions and angles defined by these proportions have this property. By definition, factor analysis yields factor vectors described by angular relationships.

Our criteria for choosing the number of mantle end-member components from our data to use in the modeling of the glass data were the following. (1) At least 95% of the variance in the data set must be explained by the sum of squares of the statistically identified end-members. (2) All modeled end-member factors that explained less than 2% of the total variance were rejected. (3) All statistically identified end-members, which did not have a coherent distribution when mapped or plotted, were rejected.

6. Statistical modeling of the MAR glass data

6.1. Spearman rank correlation coefficients (SRCCs)

We calculated the SRCCs (see Appendix A) for the MAR data set both for all of the segments combined and for each segment individually (excluding segments 4 through 6 due to small sample size). We chose to focus our interest on strong ($|\rho| > 0.80$) SRCCs significant at the 0.01 level (one-tailed). Table 2 contains the signs of the significant rank correlations for the data set. These rank relationships provide insight into the data set and afford the inspection of the data in terms of analytical consis-

Table 2
SRCCs for all segments taken together

	Ba	Ce	Eu	La	Lu	Nd	$^{143}Nd/^{144}Nd$	Pb	$^{206}Pb/^{204}Pb$	Rb	Sm	Sr	$^{87}Sr/^{86}Sr$	Th	U	Y	Yb
Ba		+		+					+	+				+	+		
Ce	+			+		+		+		+	+	+		+	+		
Eu						+					+						
La	+	+				+		+		+		+		+	+	+	+
Lu																+	+
Nd		+	+	+				+		+	+			+	+		
$^{143}Nd/^{144}Nd$									−								
Pb		+		+		+				+	+	+		+	+		
$^{206}Pb/^{204}Pb$	+						−					+		+	+		
Rb	+	+		+		+		+									
Sm		+	+			+		+									
Sr		+		+				+						+	+		
$^{87}Sr/^{86}Sr$										+							
Th	+	+		+		+		+		+		+			+		
U	+	+		+		+		+		+		+		+		+	
Y				+	+					+					+		+
Yb				+	+											+	

Deviations from these relationships among individual segments indicate the key elemental control in the end-members. The elements are in alphabetical order.

tency and to qualitatively assess the variance of the entire population. We only compare $|\rho|$ greater than 0.80 at the 0.01 significance level due to the inherent spurious correlations that arise during multiple comparison analyses. To obtain the true significance level, we divide the measured probability value by the number of comparisons (0.01/1600) giving the true significance level of 6×10^{-6}.

We compared the SRCCs on a segment-by-segment basis to identify the elemental controls related to the mantle components beneath the equatorial MAR. We do not discuss segments 4 through 6 because these segments do not have enough samples for multiple comparison. As expected, the SRCCs for the trace elements show positive correlations between incompatible elements. We use the following variables for segment-by-segment comparison based on relationships identified by the 1600 multiple comparisons (each variable to each variable) and those described by Schilling et al. (1994). We compare Ba, Ce, Eu, La, Lu, Nd, $^{143}Nd/^{144}Nd$, Pb, $^{206}Pb/^{204}Pb$, Rb, Sm, Sr, $^{87}Sr/^{86}Sr$, Th, U, Y, and Yb.

6.1.1. Northern segments

Glasses from segment 1 show significant positive correlation between La and Ba, La and $^{87}Sr/^{86}Sr$, Sr and Th, Sm and Yb. Negative correlations in these glasses include Ba and $^{143}Nd/^{144}Nd$ and Ce and $^{143}Nd/^{144}Nd$.

6.1.2. Southern segments

Of particular interest are the correlations identified in glasses from segment 7 where significant correlations between incompatible elements are rare.

The SRCCs clearly define geochemical differences between the glasses from individual segments in terms of elemental concentration and isotopic composition. These differences support the contention of mantle source heterogeneity and lay the foundation upon which further statistical treatments of the data are built. We use elements that show significant correlations (both negative and positive) to further isolate the causes of geochemical variance within the sample population.

6.2. K-means cluster analysis of the MAR segments

Based on the SRCCs described above, we selected the following variables of interest: Ce, Pb, La, Ba, Th, Sm and their respective ratios Ce/Pb, La/Ba, La/Th and $(La/Sm)_N$ and $^{206}Pb/^{204}Pb$. The variations in these ratios, as described above

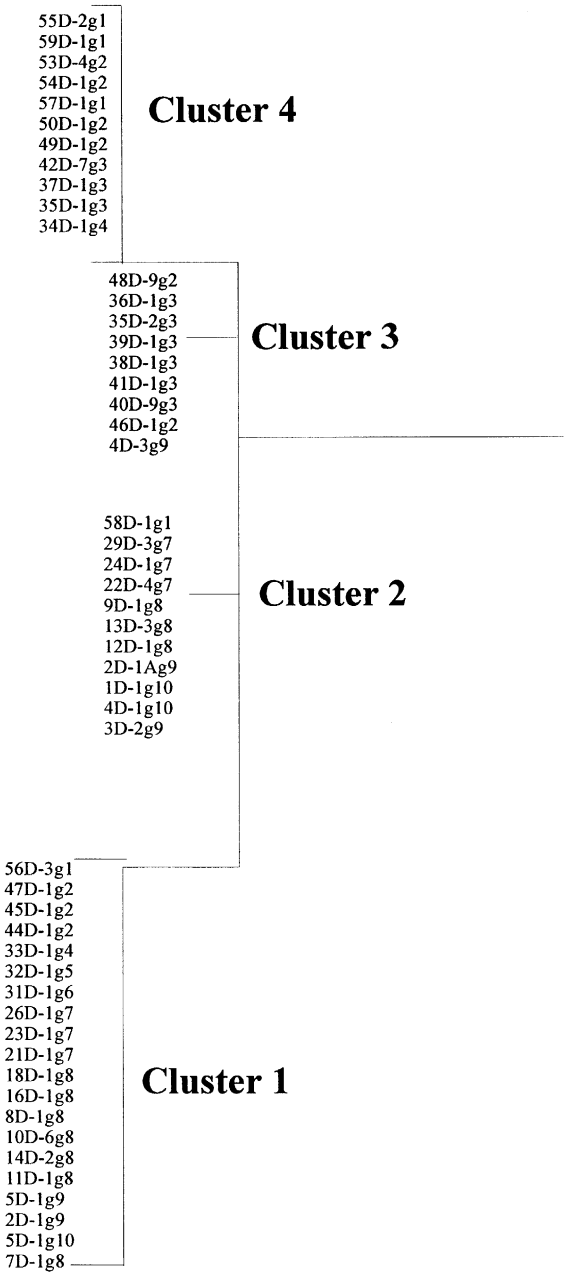

Fig. 7. Dendrogram showing the results of the K-means cluster analysis. The dendrogram shows the relatedness of samples from the different segments. For this analysis, we used the complete linkage method (Rock, 1988). The sample numbers are followed by their respective segment numbers (XD–Xg#).

define the prospective mantle end-member reservoirs beneath the equatorial MAR. The clustering procedure (see Appendix A) attempts to identify relatively homogeneous groups of cases (samples) based on selected characteristics (elements and ratios) using an algorithm that starts with each case (or sample) in a separate cluster and combines clusters until only one is left. We compared cluster membership for each sample using the above variables and the segment from which the sample came. We isolated four statistically distinct clusters. Fig. 7 shows the results of this cluster analysis. Generalization of the cluster memberships suggests that the northern segments are compositionally significantly different from samples from the southern portion of the equatorial MAR. Evidence for this lies in the absence of cluster 4 in the southern segments 5 through 10. Similarly, the dominance of cluster 1 in the south indicates heterogeneous mantle source composition. Cluster membership of segments showing evidence of mixing between end-members are described above such as in the case of samples from segment 1. These samples classify into different groups. Table 3 shows the differences between the clusters for elements used as classification variables.

Plotting the incompatible element ratios of the glasses using cluster membership rather than their ridge segment (Fig. 8), when compared to Figs. 4 and 6, shows the chemical variations of the samples grouped into geochemically contiguous clusters. Cluster analysis further identified samples which were predominantly N-MORB and HIMU types. In-

Table 3
(A) Cluster centers for the clusters identified based on trace element ratios and Pb-isotopes. (B) Distance between final cluster centers showing relative difference between each cluster

Cluster	1	2	3	4
(A)				
Ce/Pb	31.56	24.56	26.13	25.03
La/Ba	0.11	0.68	0.17	0.31
$(La/Sm)_N$	1.47	0.45	0.83	0.63
La/Th	10.46	35.17	13.7	21.52
Th/U	3.12	2.09	2.93	2.52
$^{206}Pb/^{204}Pb$	18.6	18.2	18.9	19.1
(B)				
1		8.1	6.8	8.2
2	8.1		13.9	8.4
3	6.8	13.9		9.6
4	8.2	8.4	9.6	

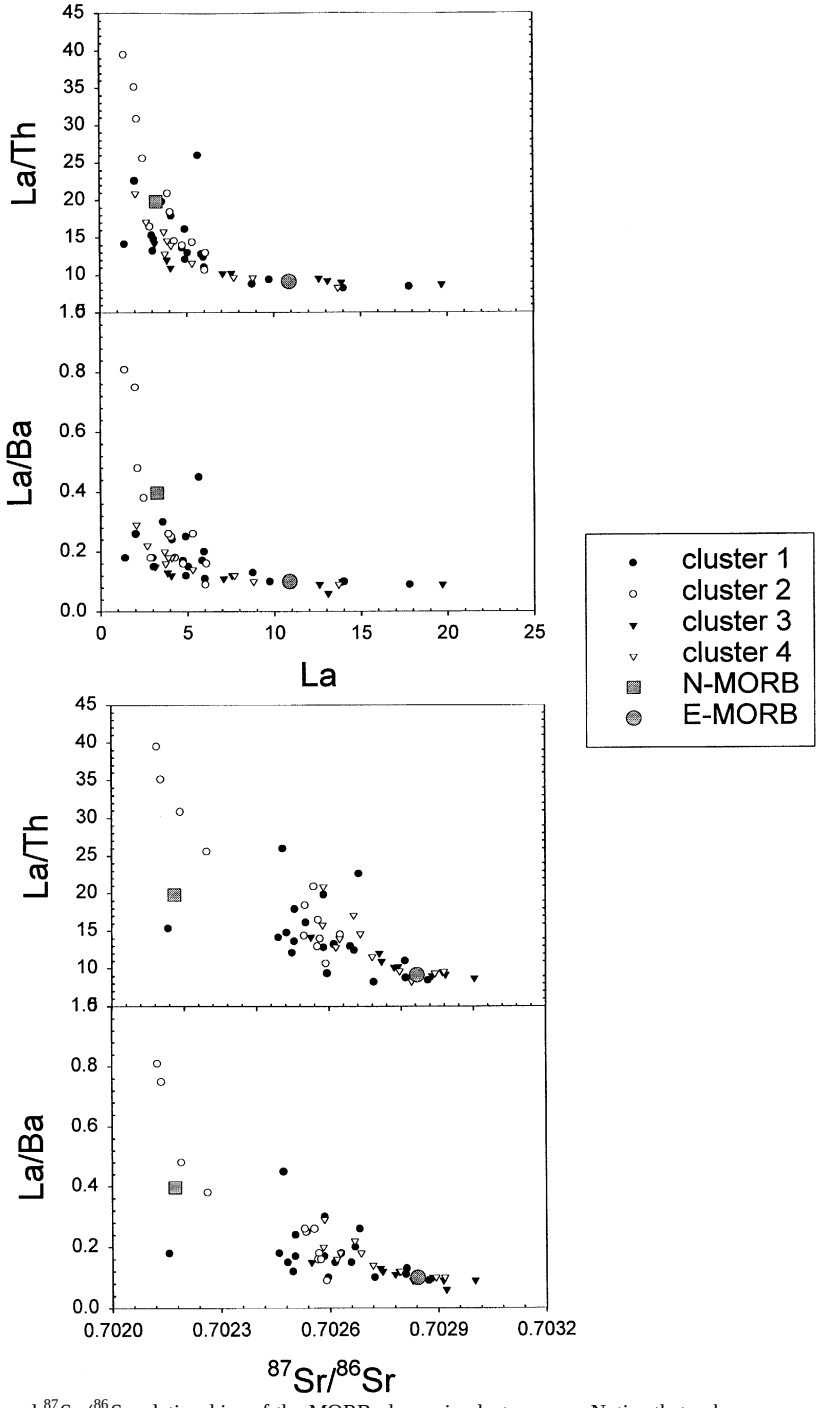

Fig. 8. La–Th, La–Ba and $^{87}Sr/^{86}Sr$ relationships of the MORB glasses in cluster space. Notice that, when compared to Figs. 4 and 6, the cluster membership clearly defines the presence of a third mantle component (cluster 1) which is delineated both geochemically and statistically.

terestingly, although statistically different, clusters 3 and 4 are remarkably similar in terms of incompatible element composition. We explore below the possibility that the statistically identified mantle reservoirs may, in fact, be an artifact of the statistical method and not geochemically viable end-member components.

6.3. Discriminant analysis of the MAR glass samples

We began the discriminant analysis (see Appendix A) using the segment numbers as a priori groups and the elements, identified by SRCCs, which geochemically segregate the samples from different segments. Using these grouping and classification variables, we found that these a priori groupings are little better at classifying the samples than "chance" with only 69% of all samples correctly classified (Table 4). This "poor" result indicates that the geochemical variation of samples from within individual segments is substantial and that samples from different ridge segments have geochemical relationships more like samples from other segments than from within their own subpopulation. To test the results of the cluster analysis, which identified four distinct clusters of samples, we ran discriminant analysis using the cluster membership to define a priori group membership. This procedure increased the correctly classified cases to 78% (Table 5).

Table 4
Classification results using the segments as a priori groups and Ba, Ce, Eu, La, Lu, Nd, $^{143}Nd/^{144}Nd$, Pb, $^{206}Pb/^{204}Pb$, Rb, Sm, Sr, $^{87}Sr/^{86}Sr$, Th, U, Y and Yb as discriminating variables

Segment	Predicted group membership										
	1	2	3	4	5	6	7	8	9	10	Total
1	1	3	0	0	0	0	0	1	0	0	5
2	1	6	2	0	0	0	0	0	0	0	9
3	0	4	5	0	0	0	0	0	0	0	9
4	0	0	0	2	0	0	0	0	0	0	2
5	0	0	0	0	0	0	1	0	0	0	1
6	0	0	0	0	0	1	0	0	0	0	1
7	0	2	0	0	0	0	4	0	0	0	6
8	1	1	0	1	0	0	0	7	0	0	10
9	0	0	0	0	0	0	0	0	5	0	5
10	0	0	0	0	0	0	0	0	0	2	2

69.0% of original grouped cases correctly classified.

Table 5
Groups correctly classified using cluster membership as a priori group

Cluster	Predicted group membership				
	1	2	3	4	Total
1	16	2	1	0	19
2	7	3	0	0	10
3	1	0	8	1	10
4	1	0	0	10	11
% 1	84.2	11	5.3	0	100
% 2	70	30	0	0	100
% 3	10	0	80	10	100
% 4	9.1	0	0	90.9	100

78.0% of original grouped cases correctly classified.

We show, statistically, that the samples classify into four subpopulations based on their trace element and isotope concentrations. We identified via SRCCs, cluster and discriminant classification that a select group of geochemical variables discriminate between the sample subpopulations. To further illustrate this fact, we again classify the samples using cluster membership with incompatible element ratios and $(La/Sm)_N$ as discriminating variables. This procedure yielded a correct classification percentage of 97.5% (Table 6). Clearly, incompatible element concentration and light-REE enrichment or depletion are the key variables in this system with each subpopulation and each sample representing the various contributions of the heterogeneous mantle end-members.

Table 6
Predicted group membership using cluster membership as the a priori group and incompatible trace element ratios and $(La/Sm)_N$ as discriminating variables

Cluster	Predicted group membership				
	1	2	3	4	Total
1	18	0	1	0	19
2	1	10	0	0	11
3	0	0	10	0	10
4	0	0	0	11	11
% 1	94.7	0	5.3	0	100
% 2	9.1	90.9	0	0	100
% 3	0	0	100	0	100
% 4	0	0	0	100	100

97.50% of original grouped cases correctly classified.

While these results, qualitatively, are not surprising, the fact that they are statistically significant indicates that they are quantifiable using extended factor analysis.

6.4. Extended Q-MODE factor analysis of the equatorial MAR glasses

Factor analysis attempts to identify the underlying or controlling factors that explain the pattern of correlations within a set of observed variables. Ideally, the data should have a bivariate normal distribution where each pair of variables and observations is independent (Norušis, 1997). Factor identification, within the factor analysis model, depends on common factors (those estimated by the model) and unique factors (those which do not overlap with observed variables). We assume that unique factors do not correlate with each other nor with the common factors. The observations in this study are inherently independent as each sample is an individual observation. We examine only those elements which are not internal to other variables. Specifically, we do not model the isotopic data since these values correlate to the parent element concentrations. We can, therefore, only characterize the mantle end-members in terms of trace element concentration. We address the normality assumption of the factor analysis model by normalizing the concentration data to a constant row-sum, as described in Eq. (12) of Appendix A, thereby closing the data.

We used the principal component algorithm to extract the factors and rotated them using varimax rotation with Kaiser normalization (Rock, 1988). We obtain the factor scores for each sample using regression along the factor vector. We performed the analyses on both the open and closed data sets; however, component composition determination uses only the closed data set results. The initial factor scores returned by the factor model for each sample are dimensionless since we normalized the original data set (Appendix A, Eq. (12)). Similarly, due to the closing of the data, the initial loadings do not sum to unity across columns. We follow the method of Miesch (1976) for deriving compositional information from the factor results as described in Eqs. (12)–(19) of Appendix A. Unlike the initial factor loadings, the compositional loadings and scores have fixed signs determined by the choice of reference axes and the nature of the compositional variation in the rocks under examination. Varimax reference axes are commonly negative but are still useful for refer-

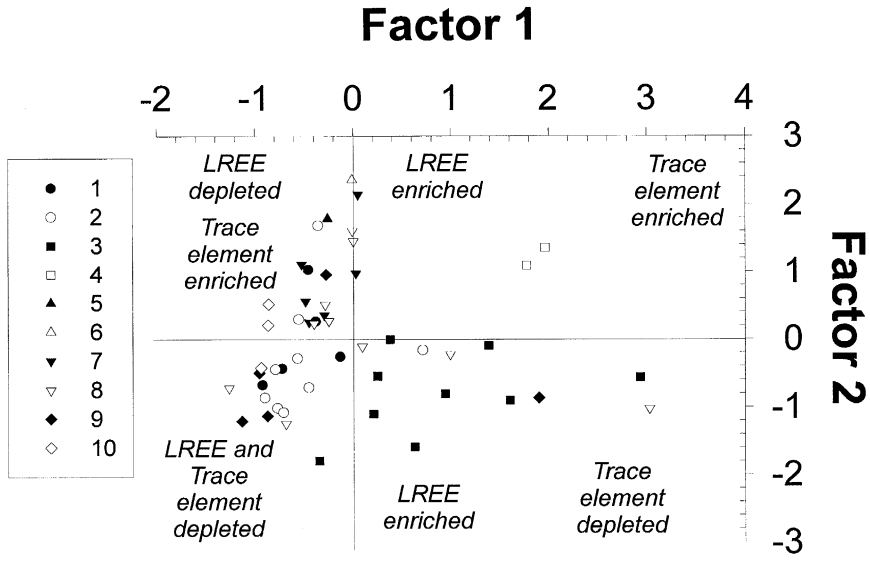

Fig. 9. Factor scores for each sample in the MAR data set. These scores are derived from the "open" data set. These results describe the nature of the components in the system based on their enrichment/depletion signatures.

ence purposes and the set of scores for each axis is still indicative of the general compositional nature of the theoretical end-members. Figs. 9 and 10 show the initial factor scores for the open and closed MAR

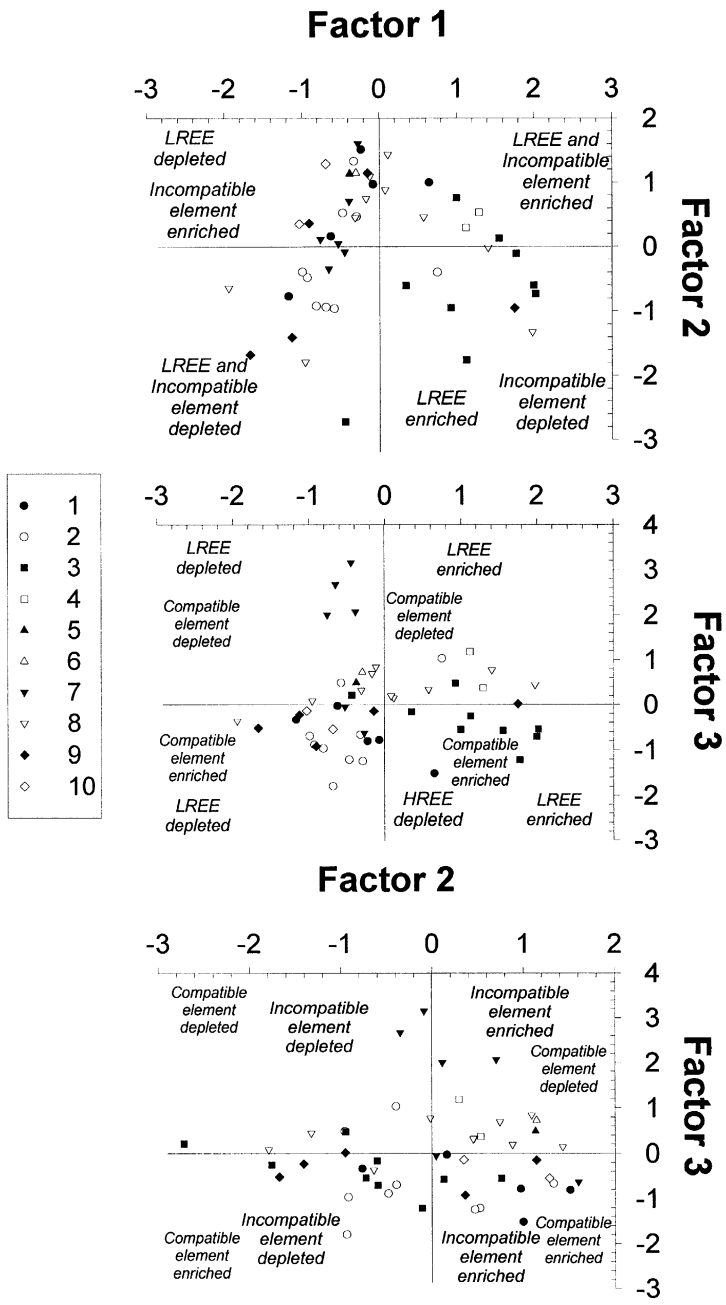

Fig. 10. Factor scores for the "closed" MAR trace element data set. The fields describe the nature of the mantle reservoirs. We show scores for factors 1 through 3. Scores for factor 4 are available by request.

data sets, respectively. (For initial and compositional scores and loadings, see Hannigan, 1997). The compositional nature of the samples falling into each field defines the basis for end-member identification. Factor 1 for both the open and closed data sets shows the degree of LREE enrichment or depletion. Refinement of factor 2 of the open data set occurs in the closed data set analysis and relates to the degree of incompatible element depletion or enrichment, particularly Th, Ba, La, Sr and Pb. Factor 3 further refines relationships defined by factor 2 of the open data analysis and is related to enrichment in heavy-REE, Y, and Rb. Table 7 compares the rotated factor scores for the open and closed data sets. Figs. 11 and 12 show the initial loadings of the elements on each factor. The loadings shown in Figs. 11 and 12 corroborate relationships defined by the SRCCs, cluster and discriminant classifications.

Table 7
Comparison of rotated factor results for (A) open and (B) closed data

	Component		
	1	2	3
(A) Rotated component			
Ba	0.957	−0.158	
Ce	0.992	0.0087	
Dy	−0.005	0.985	
Er	−0.16	0.974	
Eu	0.626	0.736	
Gd	0.1416	0.893	
Ho	−0.118	0.978	
La	0.994	−0.001	
Lu	−0.223	0.958	
Nd	0.928	0.353	
Pb	0.962	0.178	
Pr	0.973	0.212	
Rb	0.975	−0.01	
Sm	0.694	0.695	
Sr	0.935	−0.127	
Tb	0.145	0.976	
Th	0.984	−0.008	
Tm	−0.22	0.962	
U	0.985	−0.007	
Y	0.0075	0.831	
Yb	−0.22	0.957	
Extraction method: principal component analysis.			
Rotation method: varimax with kaiser normalization.			
Rotation converged in three iterations.			
(B) Rotated component matrix			
Ba	0.922	−0.267	−0.005
Ce	0.988	−0.009	0.007
Dy	−0.295	0.94	0.009
Er	−0.423	0.887	0.0067
Eu	0.564	0.71	0.279
Gd	0.285	0.893	0.259
Ho	−0.369	0.914	0.0053
La	0.978	−0.165	0.0032
Lu	−0.549	0.777	0.0076
Nd	0.956	0.193	0.142
Pb	0.934	−0.003	0.236
Pr	0.987	−0.0025	0.119
Rb	0.93	−0.265	0.0037
Sm	0.657	0.68	0.213
Sr	0.814	−0.389	0.311
Tb	−0.007	0.981	0.124
Th	0.955	−0.224	−0.0007
Tm	−0.516	0.831	0.0048
U	0.954	−0.223	0.0025
Y	−0.243	0.457	0.775
Yb	−0.54	0.799	0.0065
Extraction method: principal component analysis.			
Rotation method: varimax with kaiser normalization.			
Rotation converged in five iterations.			

The two factors identified in the open data are further refined in the closed data analysis.

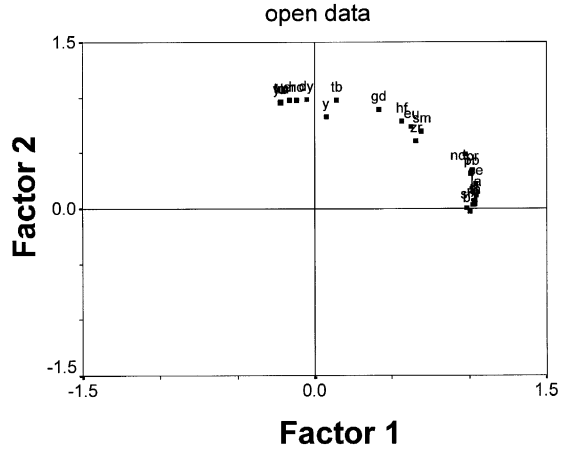

Fig. 11. Principal component plot in rotated factor space based on the “open” data set. The position of the variable in factor space shows the relative “push and pull” of each variable.

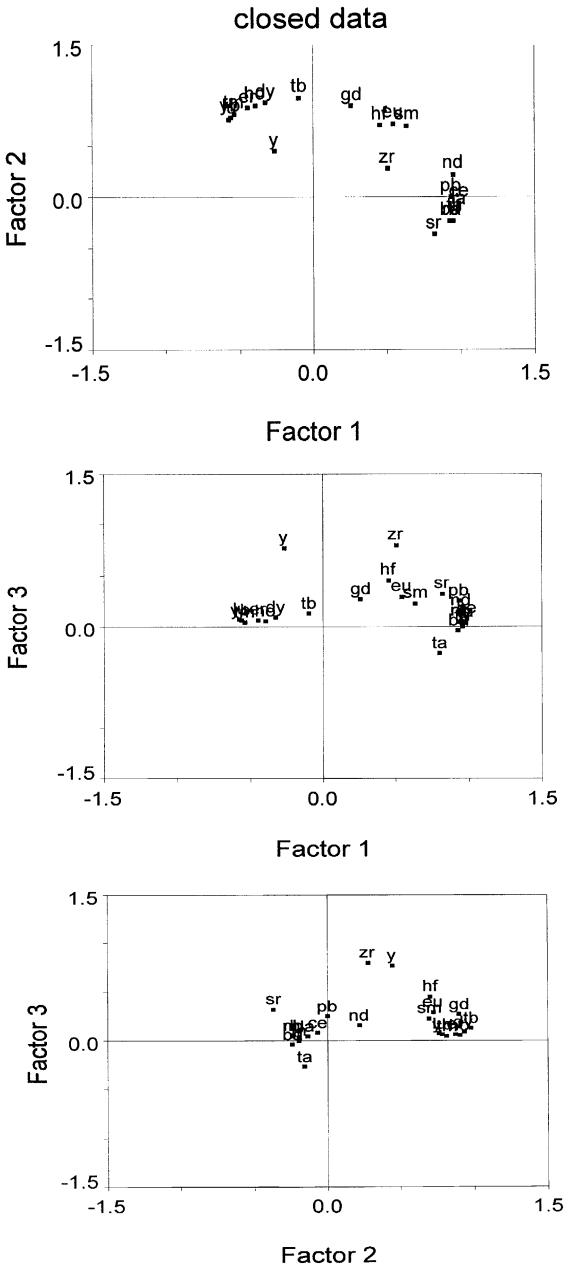

Fig. 12. Principal component plot rotated space based on the "closed" data set. Notice the relative position of the elements in factor space. A qualitative description of the population end-members can be made using these loading relationships. Again, only factors 1 through 3 are shown for clarity. Factor loadings on factor 4 are available upon request.

6.4.1. Statistically modeled end-member compositions

Using Eqs. (13)–(16) of Appendix A, we obtain compositional loadings and compositional scores for the factors. Based on the statistical results from the SRCCs, cluster analysis, discriminant analysis and factor analysis discussed above, we find four statistically distinct factors (Table 8, mantle components). The first, HIMU P-type MORB "HPM", is LREE-enriched, compatible element depleted relative to the other three identified components (see Table 8) and incompatible element-enriched. The second, depleted N-type MORB "DNM", is LREE and compatible element depleted. The third, enriched P-type MORB "EPM", is slightly LREE, incompatible element and LFSE-enriched. The fourth, transitional N-type MORB "TNM", has a flat REE pattern and is compatible element, and slightly, incompatible element depleted. The dominant end-member is DNM, which contributes the most to the variance (56.97%) in samples from all segments except segment 3. Seg-

Table 8
Modeled mantle reservoir compositions for selected trace elements and the REEs in ppm

	Factor 1 (HPM)	Factor 2 (DNM)	Factor 3 (EPM)	Factor 4 (TNM)
Rb	9.77	0.56	12.45	0.67
Sr	210.89	91.13	319.28	94.23
Y	30.16	28.13	28.12	29.45
Ba	268.30	2.33	44.08	14.28
La	24.42	2.09	7.49	4.67
Ce	44.15	6.78	17.62	12.28
Pr	4.65	1.20	2.28	1.75
Nd	18.01	8.03	10.69	9.01
Sm	3.98	2.74	3.07	2.83
Eu	1.31	1.01	1.09	1.00
Gd	4.22	3.44	3.68	3.52
Tb	0.81	0.72	0.77	0.69
Dy	4.87	4.97	4.78	4.73
Ho	1.02	1.10	1.04	1.01
Er	2.99	3.24	2.87	2.94
Tm	0.41	0.45	0.44	0.39
Yb	2.78	2.92	2.84	3.12
Lu	0.43	0.48	0.46	0.42
Pb[a]	2.11	0.31	0.59	0.47
Th	2.83	0.04	0.67	0.14
U	1.74	0.03	2.02	0.24

[a] Pb errors $\pm$ 10% because of the inclusion of Pb-isotopes in the model and the inherent violation of the independence assumption.

ment 3 shows the signature of EPM, which accounts for 2.7% of the variance of the entire data set. Segment 2 shows the influence of HPM (32.45% of total variance). Segments 7 and 8 show the strongest influence of TNM (4.5% of total variance). The average goodness-of-fit of our modeled end-member compositions is 0.98 (Appendix A, Eq. (11)) at the 0.01 significance level. Based on the relationships shown in Figs. 4, 6 and 8), we believe that the statistical identification of the fourth end-member, TNM, may, in fact, be geochemically flawed. It is clear isotopically that the third end-member, EPM, is both statistically and geochemically plausible; however, there is little if any geochemical data to support the presence of the fourth statistical end-member. We stress here the importance of agreement between statistical models and the real world and hope to clarify the value of statistical modeling in tandem with traditional data analysis (Fig. 13).

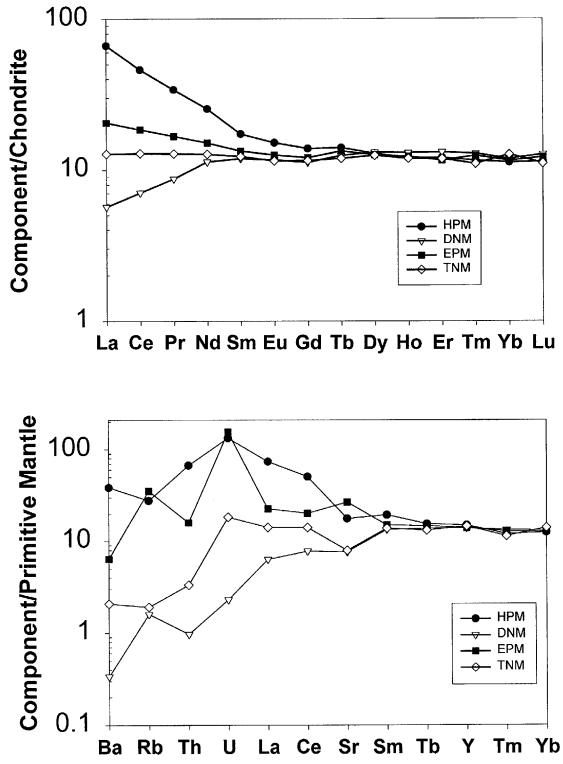

Fig. 13. Normalized REE compositions of the modeled mantle reservoirs for the 51 equatorial MAR basaltic glass samples. Component 1-EPM; Component 2-DMM; Component 3-HPM; Component 4-TNM. We plot the composition of all of the modeled components, including TNM with the understanding that geochemically this end-member is most likely a binary mixing phenomenon and not one related to a separate geochemically distinct reservoir.

6.4.2. Testing the plausibility of MAR model end-members

We used the unscaled varimax scores to find the vector representation of any given composition in the varimax space. We also used these scores to determine whether or not the composition could be that of an end-member in the compositional system. To illustrate the testing procedure, we assume that the varimax model derived from the closed data is unsatisfactory and that compositional scores for the varimax axes are not sufficiently close to those believed to exist in the MAR system. We refer to this as our "null" hypothesis H_o. We then tested literature compositions of observed, theoretical or hypothetical magma-source reservoirs as possible end-members such as E-MORB and depleted N-MORB (Sun and McDonough, 1989; Schilling et al., 1994). For simplicity, we present the factor loading for the LREE for two components only: E-MORB — La $z1_j = 10.89$, Ce $z2_j = 25.53$, Pr $z3_j = 3.17$, Nd $z4_j = 14.68$; N-MORB — La $z1_j = 2.2$, Ce $z2_j = 7.74$, Pr $z3_j = 1.30$, Nd $z4_j = 7.57$. Using Eqs. (13)–(16) in Appendix A, we derive the compositional scores from the factor loadings of the LREE (Table 8). These are E-MORB (EPM) — La $\hat{x}1_j = 7.49$, Ce $\hat{x}2_j = 17.62$, Pr $\hat{x}3_j = 2.28$, Nd $\hat{x}4_j = 10.6$;, N-MORB (DNM) — La $\hat{x}1_j = 2.09$, Ce $\hat{x}2_j = 6.78$, Pr $\hat{x}3_j = 1.2$, Nd $\hat{x}4_j = 8.03$. These compositional scores are identical to those of the modeled components EPM and DNM in Table 8.

In testing the plausibility of our statistical end-members, we continue to utilize the information concerning all four identified end-members and present a statistical model based on these mathematical results. Schilling et al. (1994) suggested that mantle end-members in the equatorial MAR include HIMU, N-type MORB and a third "orphan" component. We compared the literature compositional data for the hypothetical mantle reservoirs of HIMU P-MORB (factor 1 — HPM) depleted N-MORB (factor 2-DNM), enriched P-type MORB (factor 3 — EPM) and T-MORB (factor 4 — TNM; Langmuir et al., 1977). The equatorial MAR basaltic glass composi-

Table 9
Relative percent of factor contribution to sample composition

Sample	Segment	% HPM	% DNM	% EPM	% TNM
RC2806 55D-2g	1	21	78	0	1
RC2086 56D-3g	1	15	84	0	1
RC2086 57D-1g	1	13	85	0	2
RC2086 58D-1g	1	15	83	0	2
RC2806 59D-1g	1	24	76	0	0
RC2086 53D-4g	2	29	69	0	2
RC2086 54D-1g	2	13	87	0	0
RC2806 50D-1g	2	9	89	0	2
RC2086 49D-1g	2	9	89	0	2
RC2086 48D-9g	2	24	76	0	0
RC2086 47D-1g	2	7	92	0	1
RC2086 45D-1g	2	5	95	0	0
RC2086 44D-1g	2	8	89	0	3
RC2086 46D-1g	2	4	96	0	0
RC2086 42D-7g	3	21	79	0	0
RC2086 41D-1g	3	19	81	0	0
RC2086 40D-9g	3	17	82	0	1
RC2086 39D-1g	3	28	69	0	3
RC2086 38D-1g	3	31	67	0	2
RC2086 37D-1g	3	29	71	0	0
RC2086 36D-1g	3	38	58	0	4
RC2086 35D-1g	3	36	64	0	0
RC2086 35D-2g	3	86	14	0	0
RC2086 34D-1g	4	0	18	82	0
RC2086 33D-1g	4	0	85	15	0
RC2086 32D-1g	5	12	88	0	0
RC2086 31D-1g	6	16	84	0	0
RC2086 29D-3g	7	0	86	14	0
RC2086 26D-1g	7	0	29	0	71
RC2086 24D-1g	7	0	67	2	31
RC2086 23D-1g	7	0	73	5	22
RC2086 22D-4g	7	0	74	6	20
RC2086 21D-1g	7	0	76	0	24
RC2086 18D-1g	8	74	3	23	0
RC2086 7D-1g	8	0	18	81	1
RC2086 16D-1g	8	0	93	2	5
RC2086 8D-1g	8	0	72	22	6
RC2086 9D-3g	8	0	67	12	21
RC2086 10D-6g	8	0	78	9	13
RC2086 14D-2g	8	0	75	6	19
RC2086 11D-1g	8	0	69	5	26
RC2086 13D-3g	8	0	80	6	14

Sample	Segment	% Factor 1	% Factor 2	% Factor 3	% Factor 4
RC2086 12D-1g	8	0	75	25	0
RC2086 5D-1g	9	0	64	36	0
RC2086 4D-3g	9	0	93	7	0
RC2086 3D-2g	9	0	89	11	0
RC2086 2D-1g	9	0	45	55	0
EN061 2D-1Ag	9	0	47	53	0
RC2086 1D-1g	10	0	89	11	0
EN061 4D-1g	10	0	92	8	0
EN061 5D-1Ag	10	0	94	6	0

tions depend on the relative contribution of the end-members to the source magma. Q-MODE factor analysis allows the relative contributions of each end-member to be calculated. In general, the contributions of modeled end-members are as expected with segments 1 and 2, which show the HPM end-member with most samples being a mixture of EPM, HPM and DNM. Segment 3 samples are influenced by HPM with a small fraction of the EPM end-member. Although not modeled, samples from segment 4 are qualitatively EPM and DNM mixtures. Segments 5, 6 and 7 appear to be DNM exclusively. Segments 8 and 9 show similarities to the modeled the influence of the TNM end-member mixing with DNM and EPM. The variance accounted for by this end-member, however, can also be explained by binary mixing between EPM and DNM. Segment 10 is entirely DNM.

The result of the above modeling provide the trace element compositions of the mantle end-members of the equatorial MAR. Using the Eqs. (14)–(17), we calculated the trace element concentrations (ppm) of these four modeled end-members (Table 8). The compositions of the end-members are shown in Fig. 12. The modeled end-member compositions clearly reflect the presence of four statistically distinct magma reservoirs with substantial heterogeneity in their trace element concentrations, and ratios (e.g., La/Ba, La/Th, and Ce/Pb). The majority of glass samples show trace element signatures similar to the modeled DNM end-member. The relative proportion of each end-member in each sample is shown in Table 9. Clearly, the extended Q-MODE factor analysis technique provides significant information about the mantle end-member population beneath the equatorial MAR. Unlike inversion techniques, which also provides concentration information for the end-member population, this statistical technique provides a goodness-of-fit measure. It is this difference between standard techniques and statistical methods, which is of utmost importance in mantle end-member reservoir modeling studies.

7. Conclusions

The major contribution of factor analysis of this study is that it provides insight into the association of variance within the equatorial MAR data. The technique we employed in this study provides some objective estimates of the absolute compositions of the mantle end-member reservoirs. Although qualitative analysis of the MAR data yields information concerning possible source reservoirs and mixing components, this statistical technique provides a more objective end-member compositional data unavailable using any other technique. While this technique is not a replacement for other forms of mineralogical or geochemical (e.g., Schilling et al., 1983) data analyses, we contend that the multivariate techniques presented here provide significant information about the equatorial MAR system, which remain "invisible" to standard techniques.

Based on the trace element concentration data of equatorial MAR basaltic glasses of this study, we draw the following conclusions.

(i) The majority of samples follow the binary mixing trend between a HIMU mantle component and depleted asthenosphere. The presence of a third, geochemically distinct mantle component is seen in segments 7 and 8. The presence of this third component is best shown in the La/Th vs. La diagram (Figs. 4 and 5), which show that this third component is incompatible element depleted.

(ii) La–Th and La–Ba relationships show the relative influence of the N-MORB and HIMU end-member mantle reservoirs. These relationships corroborate the isotope results, which indicate that the Sierra Leone plume signature dominates the northernmost segments. The depleted asthenosphere reservoir dominates the southern segments. Again, the presence of a third component is suggested by the individual segment La/Th and La/Ba relationships of Figs. 4 and 5.

(iii) We have shown from our theoretical analysis of the geochemical data that the third component is, indeed, statistically distinct from N-MORB and HIMU. Although isotope data indicated its presence, the trace element relationships clearly define this third incompatible element-depleted reservoir located in the region between the Romanche and Chain fracture zones.

Based on our statistical analyses, we show the presence of four statistically distinct mantle reservoirs (Table 8) beneath the equatorial MAR system.

(iv) We identify an enriched P-type MORB end-member, showing LREE and incompatible element

enrichment. The trace element composition of this end-member is provided by our statistical model.

(v) We identify and quantify, in terms of trace element contents, the HIMU end-member, which shows significant LREE and other incompatible element enrichment.

(vi) Another statistically identified end-member is N-type MORB, showing LREE and incompatible element depletion and enriched compatible element concentrations. Our results also provide concentration data for trace elements for this reservoir.

(vii) The fourth component shows a flat REE pattern and overall incompatible element depletion. This component is also geochemically characterized by our statistical modeling of the MAR glass trace element data. The variance accounted for by this end-member can also be accounted for by simple binary mixing between DNM and EPM.

(viii) From the statistical analyses, we report in Table 9, the relative percent of each of the three main factor (reservoir) contributions to each of the 51 mid-Atlantic MORB samples. Although a fourth component is detected, its contribution to the final make up of the basalts is small. This end-member is probably a process related artifact rather than a true geochemically unique reservoir.

(ix) Finally, although these four statistical mantle end-members describe the spread in our data, the true end-member components may lay further away from the spread of the data.

Acknowledgements

This research was supported by NSF grants to A.R. Basu. We thank Drs. J.-G. Schilling, S.B. Jacobsen and K.W.W. Sims for constructive discussions concerning the content and interpretations presented in this paper. We are indebted to Dr. L. Dosso for pointing out analytical problems with some of our Ta measurements, which are excluded from this study. Dr. M.J. Bickle provided editorial comments, making us cautious in the interpretation of our geochemical data in groups as mantle end-members. We are grateful to Prof. G. Mudholkar, Department of Statistics, University of Rochester for help with the statistical modeling of the MORB glass data and to Drs. L. Dosso, and Dr. D. Fontigne and K.W.W. Sims for their thoughful and constructive reviews of this manuscript. Alfred Smith helped in the preparation of this manuscript.

Appendix A

A.1. SRCCs

To calculate SRCCs for a group of N samples containing several variables, each variable is first ranked from the highest to the lowest values using sequential integers, thus eliminating any effects of data distribution. Calculation of the measure of the correlation within the sample data set (r_s) between two variables involves the comparison of rankings from one variable to another using the following equation:

$$r_s = 1 - \frac{6\sum_{i=1}^{i=N} D_i^2}{N(N^2-1)}, \quad (1)$$

where $D_i = [\text{rank of } X_i - \text{rank } Y_i]$. The following conversion defines the significance of the r_s statistic using t-test tables:

$$t_{N-2} = r_s\sqrt{\frac{(N-2)}{(1-r_s^2)}}\,. \quad (2)$$

Perfect positive correlation ($r_s = +1$) occurs when there is a linear relationships between X and Y such that $Y_o = a + bX_i$. Perfect negative correlation ($r_s = -1$) occurs when $X_1 = Y_N$, $X_2 = Y_{N-1}$, ..., $X_N = Y_1$.

Rogers et al. (1984) provides a table detailing the measures of significance for SRCCs from various sized data sets. For a data set with $N > 30$, $|\rho|$ greater than 0.43 is significant at a = 0.01 or is out of the 99% confidence interval.

A.2. Cluster analysis

We chose hierarchical clustering to identify mantle source "groups" within our data. This technique joins the most similar observations, then successively connects the next most similar observations to these. The steps in this analysis involve the construction of

an n by n matrix of similarities between all pairs of observations and the rebuilding of the matrix by merging the samples with the highest similarities. Iteration continues by reducing the similarity matrix (n by n) to a 2 by 2 matrix. The distance coefficient (measure of similarity between samples) is defined as

$$d_{ij} = \sqrt{\frac{\sum_{k=1}^{m} \left(X_{ik} - X_{jk}\right)^2}{m}}, \quad (3)$$

where X_{ik} denotes the kth variable measured on object i, X_{jk} is the kth object measured on object j and m is the number of variables measured on each object. A criterion for clustering is that in order to link two objects to form a cluster both objects must mutually have their highest correlation with each other.

A.3. Discriminant analysis

The number of functions used to classify groups are the number of a priori groups minus one. In this study, we use the ridge segments 1 through 10 as a priori groups thereby requiring nine discriminant functions per analysis. The mean differences per variable define the construction of a discriminant function based on the group membership matrix. This matrix (D_j) is defined as:

$$D_j = \overline{A_j} - \overline{B_j} = \frac{\sum_{i=1}^{n_a} A_{ij}}{n_a} - \frac{\sum_{i=1}^{n_b} A_{ij}}{n_b}. \quad (4)$$

The differences in the pooled means ($\overline{A_j} - \overline{B_j}$, Eq. (4)) forms a vector. The next step in discriminant analysis involves the creation of a matrix of sums of squares and cross-products of all variables in group A and group B yielding a matrix of variances. Using the pooled multivariate mean vectors from Eq. (4) and the matrices of pooled variances ($[s_p^2]^{-1}$), the discriminant function becomes:

$$\left[s_p^2\right]^{-1} \cdot [D] = [\lambda]. \quad (5)$$

The set of λ coefficients in Eq. (5) enter into the discriminant function in the form:

$$R = \lambda_1\psi_1 + \lambda_2\psi_2 + \ldots \lambda_m\psi_m, \quad (6)$$

where R is the discriminant score and ψ_m is the variable (element) of interest. In our analyses, we built the distance matrix using the "Mahalanobis' distance" measure. We report the significance of this distance measure in terms of Hotelling's T^2 test.

A.4. Factor analysis

Factor analysis is a multivariate technique that expresses the total variation within a data set in terms of a number of factors. Q-MODE factor analysis identifies end-members from series of individual observations (samples). The objectives of Q-MODE factor analysis are (1) to determine the minimum number of end-members (factors) required to explain a set of data; (2) to determine the composition of these end-members A, B... in terms of the original variables (elements); (3) to describe the original objects as proportions of A, B...(aA + bB + ...), a, b being factor loadings. The Extended Q-MODE factor analysis technique scales the scores and loadings such that they sum to unity and represent end-member compositions in the units of the original data (Rock, 1988). This method is applicable to both open data (ppm) and closed data (percentage data). This method is a logical alternative to mixing models where the number of end-members is uncertain or where the end-members themselves are unknown because this statistical method tests for both cases rather than assuming the end-member compositions such as in the case of traditional binary mixing models.

Q-MODE factor analysis begins with the creation of an n by n matrix of similarities between samples. We used the cosine q coefficient of proportional similarity to build n by n matrices from the MAR data set using the equation:

$$\cos\theta_{ij} = \frac{\sum_{k=1}^{m} x_{ik}x_{jk}}{\sqrt{\sum_{k=1}^{m} x_{ik}^2 \sum_{k=1}^{m} x_{jk}^2}}. \quad (7)$$

The $\cos\theta$ value is the cosine of the angle between the two vectors defined by object i and object j in

m-dimensional space. $\cos\theta$ ranges from 1.0 (for two objects (samples) whose vector representations coincide) to 0.0 (for objects whose vectors are at 90°). The similarity matrix, which is the basis of Q-MODE factor analysis, is built by the following series of matrix algebra steps:

First, every element in every row of the data matrix is divided by the square root of the sum of squares of the elements in that row:

$$w_{ik} = \frac{x_{ik}}{\sqrt{\sum_{k=1}^{m} w_{ik} w_{jk}}}. \quad (8)$$

This step standardizes the objects so that the squares of the variables measured on each object sum to one. Then, $\cos\theta$ becomes:

$$\cos\theta_{ij} = \sum_{k=1}^{m} w_{ik} w_{jk}. \quad (9)$$

(B) In matrix algebra, the above step defines an n by n diagonal matrix [D], which contains the sums of squares of each row along the diagonal and zeros elsewhere. The standardization step in matrix becomes

$$[W] = [D]^{-\frac{1}{2}}[X] \quad (10)$$

The similarity matrix $[\cos\theta]$ in matrix form is:

$$\cos\theta = [W][W]' = [D]^{-1}[X][X]'[D]^{-1}. \quad (11)$$

Extended Q-MODE factor analysis proceeds beyond standard factor analysis by using the steps outlined by Miesch (1976) as follows. First, we transform the factor scores (unscaled scores, f''_{kj}) to the units of the original data. We closed the MAR data set using:

$$x'_{ij} = \left(x_{ij} - x\min_j\right) / \left(x\max_j - x\min_j\right), \quad (12)$$

where $x\max_j$ and $x\min_j$ are the maximum and minimum values of the jth column of the original data matrix. We "opened" the factor scores (f'_{kj}) by:

$$f_{kj} = f'_{kj}\left(x\max_j - x\min_j\right) + x\min_j. \quad (13)$$

Although Eq. (13) defines the relationship between f_{kj} and f'_{kj}, the absolute values must be established by:

$$f'_{kj} = s_k f''_{kj}, \quad (14)$$

where s_k is the scale factor:

$$s_k = \frac{K - \sum_j x\min_j}{\sum_j f''_{kj}\left(x\max_j - x\min_j\right)},$$

$$K = \sum_j x_{ij} = \sum_j f_{kj}, \quad (15)$$

and f''_{kj} is an unscaled score as defined above. In the case of factor loadings for variables (elements), the initial loadings (a''_{ik}) are transformed using Eqs. (13)–(15) substituting for a''_{ik} and a'_{ik} for f''_{kj} and f'_{kj}, respectively. The composition matrix is defined as:

$$a_{ik} = \frac{a'_{ik}}{\sum a'_{ik}}. \quad (16)$$

Quantity a_{ik} becomes the compositional loading. Since we closed the data prior to derivation of the a_{ik} and f'_{kj} matrices, the scaled scores are converted to compositional scores in order to approximate the original data using the equation:

$$\hat{x}'_{ij} = \left(x\max_j - x\min_j\right) + x\min_j$$
$$= \sum_k \left(a_{ik} f'_{kj}\left(x\max_j - x\min_j\right)\right) + x\min_j. \quad (17)$$

Based on the relationship defined in Eq. (16), it follows that $\sum a'_{ik} = 1$ so that:

$$\hat{x}'_{ij} = \left(x\max_j - x\min_j\right) + x\min_j$$
$$= \sum_k a_{ik}\left(f'_{kj}\left(x\max_j - x\min_j\right)\right) + x\min_j. \quad (18)$$

The extended Q-MODE factor model then becomes:

$$\hat{x}_{ij} = \sum_k a_{ik} f_{kj}, \quad (19)$$

where $\hat{x}'_{ij}$ refers to the reproduced original data matrix, a_{ik}'s are the compositional loadings and f_{kj}'s are the compositional scores.

References

Anders, E., Grevesse, N., 1989. Abundances of the elements: meteoritic and solar. Geochim. Cosmochim. Acta 53, 197–214.

Asmeron, Y., Jacobsen, S.B., Wernicke, B., 1994. Variations in magma source regions during large-scale continental extension, Death Valley region, Western United States. Earth Planet. Sci. Lett. 125, 235–254.

Bach, W., Erzinger, J., Dosso, L., Bollinger, C., Bougault, H., Etoubleau, J., Sauerwein, J., 1996. Unusually large Nb–Ta depletions in North Chile ridge basalts at 36°50′ to 38°56′ S: major element, trace element and isotopic data. Earth Planet. Sci. Lett. 142, 223–240.

Basu, A.R., Faggart, B.E., 1996. Temporal isotopic variations in the Hawaiian mantle plume: the Lanai anomaly, the Molokai fracture zone and a seawater-altered lithospheric component in Hawaiian volcanism. In: Basu, A.R., Hart, S.R. (Eds.), Earth Processes: Reading the Isotopic Code. Geophys. Monogr. 95, Am. Geophys. Union, pp. 149–159.

Chayes, F., 1960. On correlation between variables of constant sum. J. Geophys. Res. 65, 4185–4193.

Chayes, F., Kruskal, W., 1966. An approximate statistical test for correlations between proportions. J. Geol. 74, 692–702.

Davis, J.C., 1986. Statistics and Data Analysis in Geology. Wiley, New York.

Dosso, L., Bougault, H., Joron, J.L., 1993. Geochemical morphology of the north mid-Atlantic Ridge 10°–24°N: trace element–isotopes complimentarity. Earth Planet. Sci. Lett. 120, 443–462.

Dosso, L., Bougault, H., Langmuir, C., Bollinger, C., Bonnier, O., Etoubleau, J., 1999. The age and distribution of mantle heterogeneity along the mid-Atlantic Ridge (31–10°N). Earth Planet. Sci. Lett. 170, 169–286.

Fontignie, D., Schilling, J.-G., 1991. $^{87}Sr/^{86}Sr$ and REE variations along the Easter Microplate boundaries (south Pacific): application of multivariate statistical analyses to ridge segmentation. Chem. Geol. 89, 209–241.

Forsythe, L.M., Nielsen, R.L., Fisk, M.R., 1994. High-field-strength element partitioning between pyroxene and basaltic to dacitic magmas. Chem. Geol. 117, 107–125.

Hanan, B.B., Kingsley, R.H., Schilling, J.-G., 1986. Pb isotope evidence in the South Atlantic for migrating ridge-hotspot interactions. Nature 322, 137–144.

Hannigan, R.E., 1997. Trace and Major Elements in Sedimentary and Igneous Processes: REE Geochemistry of Black Shales and MORB and Major Element Chemical Variations in Plume-Generated Basalts. PhD thesis, University of Rochester, New York.

Hart, S.R., Zindler, A., 1989. Constraints on the nature and development of chemical heterogeneities in the mantle. In: Peltier, W.R (Ed.), Mantle Convection. Gordon & Breach, New York, pp. 261–387.

Hollocher, K., 1993. Geochemistry and origin of volcanics in the Ordovician Partridge formation, Bronson Hill Anticlinorium, west-central Massachusetts. Am. J. Sci. 293, 671–721.

Humphries, S.E., Thompson, G., Schilling, J.-G., Kingsley, R.H., 1985. Petrological and geochemical variations along the mid-Atlantic Ridge between 46°S and 32°S: influence of the Tristan da Cunha mantle plume. Geochim. Cosmochim. Acta 49, 1445–1464.

Johnson, K.T.M., Fisk, M.R., Naslund, H.R., 1995. Silicate melt inclusions from ODP Leg 140 diabases: petrogenetic implications. Eos (Trans. Am. Geophys. Union) 76, 267 (abstract).

Klein, E.M., Langmuir, C.H., 1987. Global correlations of ocean ridge basalt chemistry with axial depth and crustal thickness. J. Geophys. Res. 94, 8089–8115.

Kurz, M.D., 1993. Mantle heterogeneity beneath ocean islands: some inferences from isotopes. In: Cox, K.G., McKenzie, D.P., White, R.S. (Eds.), Melting and Melt Movement in the Earth. Royal Society, Oxford Univ. Press, Oxford, United Kingdom, pp. 91–103.

Langmuir, C.H., Bender, J.F., Bence, A.E., Hanson, G.N., 1977. Petrogenesis of basalts from the Famous area: mid-Atlantic Ridge. Earth Planet. Sci. Lett. 36, 133–156.

Leinen, M., Pisias, N., 1984. An objective technique for determining end-member compositions and for partitioning sediments according to their sources. Geochim. Cosmochim. Acta 48, 47–62.

Leinen, M., Stakes, D., 1979. Metal accumulation rates in the central equatorial Pacific during Cenozoic time. Geol. Soc. Am. Bull. 90, 357–375.

McDonough, W., 1998. Earth's core, In: Marshall, C.P., Fairbridge, R.W. (Eds.), The Encyclopedia of Geochemistry Kluwer Academic Publishing, London.

McDonough, W.F., Sun, S.S., 1995. The composition of the Earth. Chem. Geol. 120, 223–253.

McKenzie, D., O'Nions, R.K., 1991. Partial melt distributions from inverse of rare earth element concentrations. J. Petrol. 32, 1021–1091.

McMurty, G.W., Veeh, H.H., Moser, C., 1981. Sediment accumulation rate patterns on the northwestern Nazca Plate. In: Klum, L.D. (Ed.), Nazca Plate: Crustal Formation and Andean Convergence. Geol. Soc. Am., Boulder, CO, pp. 211–249.

Michael, P. et al., 1995. Regionally distinctive sources of depleted MORB: evidence from trace elements and H_2O. Earth Planet. Sci. Lett. 131, 301–320.

Miesch, A.T., 1976. Q-mode factor analysis of geochemical and petrologic data matrices. Statistical Modeling in Field Geochemistry. USGS Professional Paper 574G.

Niu, Y., Batiza, R., 1995. Extreme mantle source heterogeneities beneath the northern East Pacific Rise — trace element evidence form near ridge seamounts. Eos (Trans. Am. Geophys. Union) 76, 595.

Norušis, M.J., 1997. SPSS version 7.5, Professional Statistics. SPSS, Chicago.

Rock, N.M.S., 1988. Numerical geology, Lect. Notes Earth Sci. vol. 18. Springer-Verlag, New York.

Rogers, P.J., Stea, R.R., MacDonald, M.A., 1984. Statistical Investigation of the geochemical reflection of Au mineralization in the tills and lake sediments of the Eastern Shore of Nova Scotia. In: Jones, M.J. (Ed.), Prospecting in Areas of Glaciated Terrain. Institution of Mining and Metallurgy, London, pp. 137–152.

Saunders, A.D., Tarney, J., 1984. Geochemical characteristics of basaltic volcanism with back-arc basins. In: Kokelaar, B.P., Howells, M.F. (Eds.), Marginal Basin Geology. Geological Society of London, London, pp. 59–76.

Schilling, J.-G., 1991. Fluxes and excess temperatures of mantle plumes inferred from their interaction with migrating mid-ocean ridges. Nature 352, 397–403.

Schilling, J.-G., Zajac, M., Evans, R., Johnston, T., White, W., Devine, J.D., Kingsley, R., 1983. Petrologic and geochemical variations along the mid-Atlantic Ridge from 29°N to 73°N. Am. J. Sci. 283, 510–586.

Schilling, J.-G., Hanan, B.B., McCully, B., Kingsley, R.H., 1994. Influence of the Sierra Leone mantle plume on the equatorial mid-Atlantic Ridge: a Nd–Sr–Pb isotopic study. J. Geophys. Res. 99, 12005–12028.

Sims, K.W.W., DePaolo, D.J., 1997. Inferences about mantle magma sources form incompatible element concentration ratios in oceanic basalts. Geochim. Cosmochim. Acta 61, 765–784.

Snow, J.E., Hart, S.R., Dick, H.J.B., 1993. "Orphan" ^{87}Sr in abyssal peridotites: daddy was a granite. Science 262, 1861–1863.

Stanley, C.R., 1990. Descriptive statistics for *N*-dimensional closed arrays: a spherical coordinate approach. Math. Geol. 22, 933–955.

Sun, S.-S., 1980. Lead isotopic study on young volcanic rocks from mid-ocean ridges, ocean islands and island arcs. Philos. Trans. R. Soc. London, Ser. A 297, 409–445.

Sun, S.-S., McDonough, W.F., 1989. Chemical and isotopic systematics of oceanic basalts: implications for mantle composition and processes. In: Saunders, A.D., Norry, M.J. (Eds.), Magmatism in Ocean Basins. Geological Society of London, pp. 313–345.

Tatsumoto, M., Knight, R.J., Delevaux, M.H., 1972. Uranium, thorium, and lead concentrations in three silicate standards and a method of lead isotopic analysis, U.S.G.S. Prof. Paper, pp. D111–D115.

Teichmann, F., 1995. Sr–Nd isotopes and trace element geochemistry as petrogenetic and geochronologic indicators of lithospheric evolution. Unpublished PhD thesis, University of Rochester, Rochester.

Watson, S., McKenzie, D., 1991. Melt generation by plumes: a study of Hawaiian volcanism. J. Petrol. 32, 501–537.

Watson, S., 1993. Rare earth element inversion and percolation models for Hawaii. J. Petrol. 34, 763–783.

Wilson, M., 1989. Igneous Petrogenesis: A Global Tectonic Approach. Harper Collins, London.